BRNO UNIVERSITY OF TECHNOLOGY
VYSOKÉ UČENÍ TECHNICKÉ V BRNĚ

FACULTY OF CHEMISTRY
FAKULTA CHEMICKÁ

INSTITUTE OF PHYSICAL AND APPLIED CHEMISTRY
ÚSTAV FYZIKÁLNÍ A SPOTŘEBNÍ CHEMIE

PREPARATION AND CHARACTERISATION OF ENCAPSULATED BIOGENIC NANOPARTICLES FOR MEDICAL APPLICATION

PŘÍPRAVA A CHARAKTERIZACE ENKAPSULOVANÝCH BIOGENNÍCH NANOČÁSTIC PRO MEDICÍNSKÉ APLIKACE

BACHELOR'S THESIS
BAKALÁŘSKÁ PRÁCE

AUTHOR — **Veronika Poláková**
AUTOR PRÁCE

SUPERVISOR — **Ing. Jana Brtníková, Ph.D.**
VEDOUCÍ PRÁCE

BRNO 2020

BRNO UNIVERSITY OF TECHNOLOGY
FACULTY OF CHEMISTRY

Specification Bachelor's Thesis

Project no.:	FCH-BAK1530/2019	Academic year:	2019/20
Department:	Institute of Physical and Applied Chemistry		
Student:	**Veronika Poláková**		
Study programme:	Chemistry and Chemical Technologies		
Study branch:	Chemistry for Medical Applications		
Head of thesis:	**Ing. Jana Brtníková, Ph.D.**		

Title of Bachelor's Thesis:

Preparation and characterisation of encapsulated biogenic nanoparticles for medical application

Bachelor's Thesis:

1) Literature review concerning encapsulation of antibacterial biogenic nanoparticles with intended use in medicine.
2) Preparation and encapsulation of biogenic antibacterial nanoparticles.
3) Investigation of the effect of encapsulation on physico–chemical properties of nanoparticles.
4) Evaluation and interpretation of results.
5) Conclusion.

Deadline for Bachelor's Thesis delivery: 31.7.2020:

Bachelor's Thesis should be submitted to the institute's secretariat in a number of copies as set by the dean This specification is part of Bachelor's Thesis

Veronika Poláková Student	Ing. Jana Brtníková, Ph.D. Head of thesis	prof. Ing. Miloslav Pekař, CSc. Head of department

In Brno dated 31.1.2020

prof. Ing. Martin Weiter, Ph.D.
Dean

ABSTRACT

The aim of this bachelor thesis is a preparation and polymeric encapsulation of antibacterial biogenic nanoparticles in order to enhance their stability, reduce possible cytotoxicity while maintaining antibacterial activity. The theoretical part contains an overview of regenerative medicine, commonly used nanostructures in regenerative medicine, their properties, and methods of encapsulation. The experimental work especially focuses on selenium nanoparticles synthesis using different methods with specific protecting agents followed by encapsulation via nature-inspired polymer. The used encapsulation methods are based on self-assembly polymerization and coating of selected natural polymeric adhesive. The chemical and physical properties of pure and encapsulated selenium nanoparticles, such as their concentration and morphology (size and shape) were studied using Fourier-transformed infrared spectrophotometry and scanning transmission electron microscopy. It was found that different used method provides nanoparticles with different size, shape and stability. As a main result, an optimized method of selenium particles synthesis, stabilization and encapsulation was developed and described. Nanoparticles, synthesized using this method, are spherical with size ranging from 10.5 to 101 nm. The sizes of most of the synthesized nanoparticles lay within 10.5 to 40 nm interval. When encapsulated, their sizes increase and are ranging from 74.5 to 571.5 nm.

KEYWORDS

Regenerative medicine, encapsulation, selenium nanoparticles, nanostructures, antibacterial, biogenic, polymerization, self-assembly.

ABSTRAKT

Cieľom tejto bakalárskej práce je príprava a polymérová enkapsulácia antibakteriálnych biogénnych nanočastíc, tak aby sa zvýšila stabilita, znížila cytotoxicita a bola zachovaná ich antibakteriálna aktivita. Teoretická časť obsahuje informácie o regeneratívnej medicíne, bežne používaných nanoštruktúrach v regeneratívnej medicíne, ich vlastnostiach a metódach enkapsulácie. Experimentálna časť popisuje procesy prípravy selénových nanočastíc za použitia rôznych metód so špecifickými stabilizátormi a pokračuje enkapsuláciou do prírodného polyméru. Použité metódy enkapsulácie sú založené na samostatnej polymerizácii a pokrývaní vybraným, v prírode sa vyskytujúcim polymérom s adhezívnymi vlastnosťami. Boli skúmané chemické a fyzikálne vlastnosti čistých a enkapsulovaných selénových nanočastíc, ako je ich koncentrácia a morfológia (veľkosť a tvar), boli skúmané pomocou infračervenej spektrofotometrie s Fourierovou transformáciou a skenovacej transmisnej elektrónovej mikroskopie. Bolo zistené, že rôzne metódy poskytnú nanočastice s rôznou veľkosťou, tvarom a stabilitou. Hlavným výsledkom je vytvorenie a popísanie optimalizovanej metódy syntézy selénových častíc, ich stabilizácia a enkapsulácia. Nanočastice syntetizované touto metódou majú sférický tvar a ich veľkosť sa pohybuje v rozmedzí od 10.5 do 101 nm. Veľkosť väčšiny takto syntetizovaných nanočastíc leží v intervale od 10.5 do 40 nm. Enkapsulované nanočastice sú väčšie a pohybujú sa v hodnotách od 74.5 do 571.5 nm.

KĽÚČOVÉ SLOVÁ

Regeneratívna medicína, enkapsulácia, selénové nanočastice, nanoštruktúry, antibakteriálne, biogénne, polymerizácia, samostatná.

POLÁKOVÁ, Veronika. *Příprava a charakterizace enkapsulovaných biogenních nanočástic pro medicínské aplikace.* Brno, 2020. Dostupné také z: https://www.vutbr.cz/studenti/zav-prace/detail/124172. Bakalářská práce. Vysoké učení technické v Brně, Fakulta chemická, Ústav fyzikální a spotřební chemie. Vedoucí práce Jana Brtníková.

DECLARATION

I declare that the diploma/bachelor thesis has been worked out by myself and that all thequotations from the used literary sources are accurate and complete. The content of the diploma/bachelor thesis is the property of the Faculty of Chemistry of Brno University of Technology and all commercial uses are allowed only if approved by both the supervisor and the dean of the Faculty of Chemistry, BUT.

.....
student's signature

Acknowledgments:

I would like to thank my supervisor Ing. Jana Brtníková, Ph.D. for valuable advises, Ing. Jana Dorazilová for creation of good work conditions, English correction and help during the experiments and all colleagues involved in this work. I would like to thank Ing. Petr Sedláček, Ph.D. for FTIR measurement. Also, I would like to thank my family and friends for their support.

CONTENT

1 INTRODUCTION 8

2 STATE OF THE ART 9

2.1 Regenerative Medicine and Tissue Engineering 9

2.1.1 Additives to Enhance Regenerative Potential of Biomaterials 9

2.2 Nanostructures and Regenerative Medicine 11

2.3 Antibacterial Nanoparticles 15

2.3.1 Traditionally Used Antibacterial Nanoparticles 15

2.3.2 Biogenic Antibacterial Nanoparticles 18

2.4 Selenium Nanoparticles 19

2.4.1 Preparation of Selenium Nanoparticles 20

2.4.2 Potential Cytotoxicity of Selenium Nanoparticles 21

2.5 Encapsulation as a Method for Designing Nanoparticles with Specific Parameters 21

2.5.1 Methods of Encapsulation 21

2.6 Dopamine 22

2.6.1 Self-polymerization of Dopamine 22

2.6.2 Encapsulation of Nanoparticles in Polydopamine 23

3 GOAL OF THE WORK 26

4 EXPERIMENTAL PART 27

4.1 Material and equipment 27

4.1.1 Chemicals 27

4.1.2 Instruments 27

4.2 Preparation of selenium nanoparticles 27

4.2.1 Selenium nanoparticles stabilized by chitosan 27

4.2.2 Selenium nanoparticles stabilized by poly (sodium 4-styrenesulfonate) 28

4.2.3 Washout and re-dispersion of selenium nanoparticles 28

4.3 Physicochemical characterization of selenium nanoparticles 28

4.3.1 Concentration determination of selenium nanoparticles stabilized by chitosan 28

4.3.2 Concentration determination of selenium nanoparticles stabilized by poly (sodium 4-styrenesulfonate) 28

4.3.3 Morphology and size evaluation 29
4.3.4 Chemical structure characterisation 29
4.4 Encapsulation by pH-induced self-polymerization of dopamine 29
4.4.1 Encapsulation method I 29
4.4.2 Encapsulation method II 31
4.4.3 Washout and re-dispersion of encapsulated selenium nanoparticles 32
4.5 Physicochemical characterization of encapsulated selenium nanoparticles 33
4.5.1 Morphology and size evaluation 33
4.5.2 Chemical structure characterization 33
5 RESULTS AND DISCUSSION 34
5.1 Characterization of selenium nanoparticles 34
5.1.1 Concentration determination of selenium nanoparticles stabilized by chitosan 34
5.1.2 Concentration determination of selenium nanoparticles stabilized by poly (sodium 4-styrenesulfonate) 34
5.1.3 Morphology and size evaluation 36
5.1.4 Chemical structure characterization 40
5.2 Encapsulation by pH-induced self-polymerization of dopamine 42
5.2.1 Morphology and size evaluation 43
5.2.2 Chemical structure characterization 52
6 CONCLUSION 57
7 REFERENCES 58
8 LIST OF ABBREVIATIONS 65
9 LIST OF FIGURES 66
10 LIST OF TABLES 68

1 INTRODUCTION

Regenerative medicine is a rising multidisciplinary field of science focusing on regeneration or replacement of malfunctioned damaged tissue using novel approaches of applying biocompatible materials, nanotherapeutics strategies, cellular therapies, and protein signalization both alone and combined to achieve said purpose.

In recent years, nanoparticles became a very popular objects of studies amongst researches for their unusual properties, such as antimicrobial activity. However, their use for the purposes of regenerative medicine is limited by their stability and toxicity in a physiological environment. Stabilization of nanoparticles using encapsulation processes is one of the ways how to conquer these complications. Encapsulation is nowadays widely used in cosmetics, drug delivery systems, food industry, pesticides, and textiles. In many cases, it can improve the stability and biocompatibility of nanoparticles.

This bachelor thesis deals with the selenium nanoparticles synthesis, stabilization and encapsulation with polydopamine self-assembly. Nanoparticles size, morphology and stability are characterized and discussed.

2 STATE OF THE ART

2.1 Regenerative Medicine and Tissue Engineering

Regenerative medicine is known as a wide multidisciplinary field of science, which is expected to cure various human illnesses. It especially deals with maintenance, restoration, regeneration, and enhancement of tissues. It is a promising way of how to treat both chronic diseases and acute injuries by providing scaffolding material or bioactive substances to induce regeneration.[1],[2] Thus the regenerative medicine is a possible future for medicine, treating the tissue damage whilst avoiding transplantation or other destructive means of traditional medicine.[2] Nowadays, regenerative medicine is divided into three distinctive fields - cell signaling, gene therapy, and tissue engineering.[3],[4] As the main field of regenerative medicine, tissue engineering strives to develop functional materials with regenerative potential thus connecting all three areas as well as stands alone as a group. Such materials can be future for non-invasive transplantation surgery as well as create a sufficient environment for studying cellular behavior *in vitro*.[5]

2.1.1 Additives to Enhance Regenerative Potential of Biomaterials

When it comes to the application of the material, level of cytotoxicity, biodegradability, biocompatibility, active surface area and durability determine if the material has the application potential for tissue engineering.[6] Suitability of the material is determined by the type of the regenerated tissue as well. Metals, polymers, ceramics, and composites of the above mentioned can be used for tissue regeneration. Magnesium and titanium are commonly used metals. Zirconia oxides, alumina oxides, calcium phosphates, or bioactive glass fall within bioceramics group.[7] Polymers are widely used in scaffold preparation, due to their practical features, such as a large surface area in comparison to its volume, amount and size of pores, biocompatibility, etc. Polymers can be either naturally extracted or artificially prepared. Collagen is a classic example of a commonly used biopolymer with wide natural occurrence. Besides collagen, there are many naturally derived polymers, regularly used, such as gelatine, chitosan, chitin, cellulose, starch, and others. Popular artificially acquired polymers are poly(lactic acid), poly(glycolic acid), poly(lactic-co-glycolic acid) etc.[6] In general, composite materials are prepared as an arbitrary combination of previously mentioned material groups. Flow chart for the classification of biomaterials, which are described above, is shown in Figure 1.

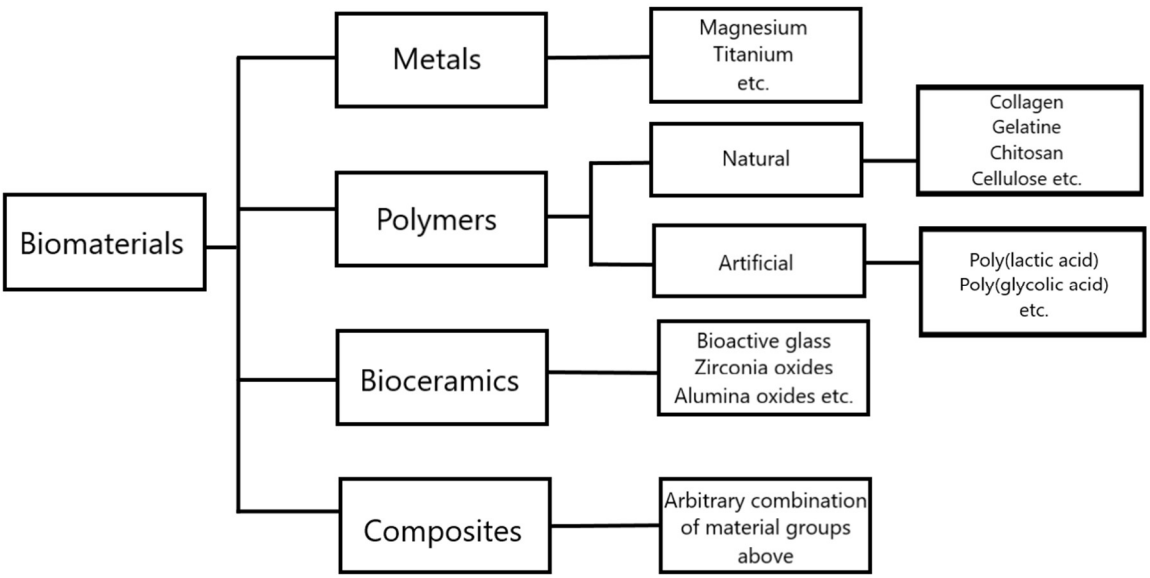

Figure 1: Flow chart for the classification of biomaterials with examples.

Every group of biomaterials has its field of application and its advantages and disadvantages. Usually, materials undergo further modification either to their surface or whole volumes to ensure the highest cytocompatibility as possible. Additives can offer many positive improvements of the material, such as enhancing adhesion, antimicrobial properties, anti-inflammatory activity, tissue regeneration, mineralization, cell proliferation, etc. The rigidity of metals finds its use in bone tissue reconstruction. To prevent metal's toxic corrosive effect, the surface is modified by ceramic coatings. Bioceramics are used as the tissue replacements, if the hard tissue is polluted or damaged, due to its better tolerance with surrounding tissues. Biopolymers and synthetic polymers can be modified by synthetic addition of hydrophilic groups or by surface modification with bioactive additives.[7] Zinc can bring antimicrobial activity to the material, silicone boosts cell growth, and adhesion.[8] The following table summarize the spectrum of used additives in tissue regeneration.

Table 1: Summarisation of additives used in tissue regeneration.

Modification	Additive	Biomaterial	Reference
Adhesion	Hydroxypropyl pea starch	Soluplus® films	[9]
	Usnic acid	Carboxymethyl cellulose-polypyrrolidine-carbopol 971 films	[10]
Biomechanics	Clay minerals	poly(N-isopropylacrylamide) hydrogel	[11]
	Fluorapatite-based glasses	Polyvinylalcohol-polyurethan foams	[12]
Wound healing	Calciferol (vitamin D3)	Tetraethyl orthosilicate based bio-glass scaffold	[13]
	Strontium	Polyvinylalcohol-polyurethan foams	[14]
	Antibacterial peptides	Ureido-pyrimidinone films	[15]
Antibacterial properties	Resveratrol	Polyvinylalcoho-chitosan films	[16]
	Usnic acid	Carboxymethyl cellulose-polypyrrolidine-carbopol 971 films	[17]

2.2 Nanostructures and Regenerative Medicine

Nanostructured materials are structures, systems, devices with unusual, novel, or enhanced properties caused by their small dimensions. Dimensions of the nanostructures range between 1 and 100 nm.[8] Nanotechnology, the field of science dealing with nanostructures, attempts engineering of low-dimensional structures by two approaches. The “bottom-up” approach fabricates the nanostructures from atoms or molecular constituents using assembly or self-assembly procedures. In some resources, the term “molecular nanotechnology” or “molecular manufacturing” is commutable for the “bottom-up” approach.[18] The “top-down” approaches are based on disintegration or reduction of bigger-sized structures to nanoscale and so-prepared nanostructures usually maintain their old properties.[19] In nanoscale, the physical, chemical, and biological properties deviate depending on the size/volume ratio and the shape of the nanoparticles.[20], [21] Nanostructures can exist in many different shapes such as spheres, fibers, cylinders, tubes, and many others [22]. The surface of the nanostructures can be modified as well, to be better suited for their application. The size of structures has a huge impact on physical, electronic, magnetic, and optical properties.[23]

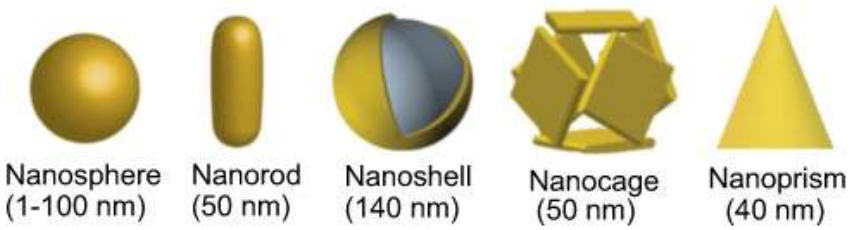

Figure 2: Schematic illustration of nanostructure shapes [24].

The existence of nano-sized materials offers novel possibilities for material modifications improving mechanical, conductive, optical, and antibacterial properties as well as work as a controlled drug delivery systems.[25] For example, a study published in 2009, aimed to design a functional scaffold which could be used for rotator cuff reparation and augmentation. The rotator cuff is a very complicated body part, consisting of four muscles and tendons. Most shoulder injuries are located here. Because of its complex anatomy, it is very difficult to repair. This study discusses possible ways of nanofiber incorporation into a scaffold, to provide better mechanical properties. In conclusion, the aligned and unaligned nanofiber scaffold made a big change in rotator cuff fibroblast response and can change the rotator cuff healing processes. The aligned scaffold, used *in vitro*, maintained its mechanical properties.[26]

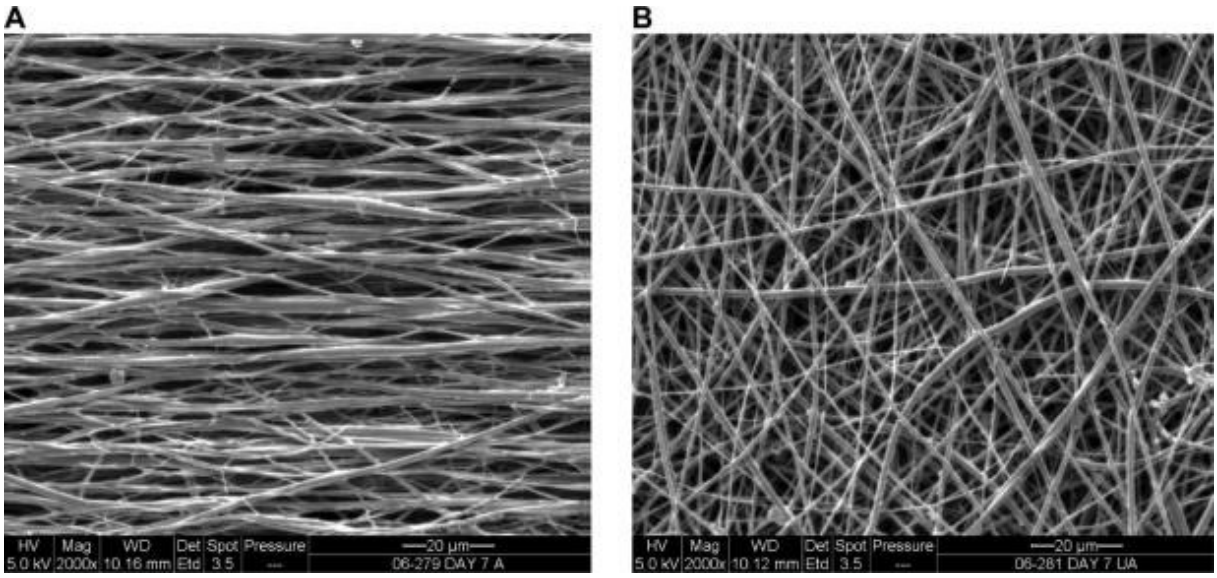

Figure 3: SE images of aligned (A) and unaligned (B) nanofiber scaffolds [26].

Another study, by Qian *et al*, also deals with scaffolds used in regenerative medicine. It aims to create an electrophysiological carbon nanotube gel scaffold via the specific pairing of functionalized nucleobases, which can be applied in drug delivery and can speed up *in vitro* osteogenesis. The gel scaffold was achieved by the Watson-Crick base pairing between thymine and adenine, which is formed via hydrogen bonding. For the pairing heparin, a negatively charged glycosaminoglycan was functionalized with adenine and thymine. The preparation process is described in Figure 4. It is commonly used as an anticoagulant. It was observed that,

when added into a biopolymer, the carbon nanotube gel scaffold significantly affected the electrophysiological and mechanical properties. Scaffold conductivity, compression modulus, and biocompatibility were dependent on the concentration of carbon nanotube gel. The scaffolds in combination with electrical stimulate provided spontaneous and strong osteogenesis.[27]

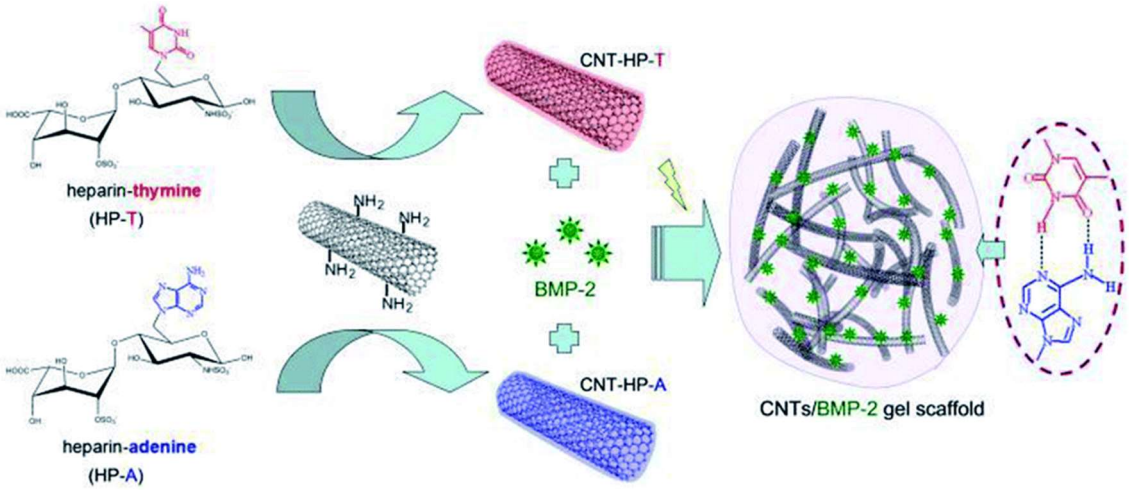

Figure 4: Schematic illustration of the carbon nanotube gel scaffold preparation [27].

The Study of Gabay *et al* deals with engineering, electrically conductive neuronal networks, which are formed by ganglion-like clusters of neurons. In this study, high-density carbon nanotube templates were used, to enhance spot adherence properties and to form well defined, cultured neuronal clusters on it. This is performed by photolithography, micro-contact printing, and nanotube chemical vapor deposition techniques. The carbon nanotube islands are shown in Figure 5. The neuron cell moves on low-affinity substrate to spots with higher affinity, which are provided by carbon nanotubes. The neuron cells stick to the spot and gather there. The process is not difficult and offer a wide range of substrates, that can be used. The neuron cluster formation is stable, using this self-assembly method.[28] The progress of neuronal systems formation is shown in Figure 6.

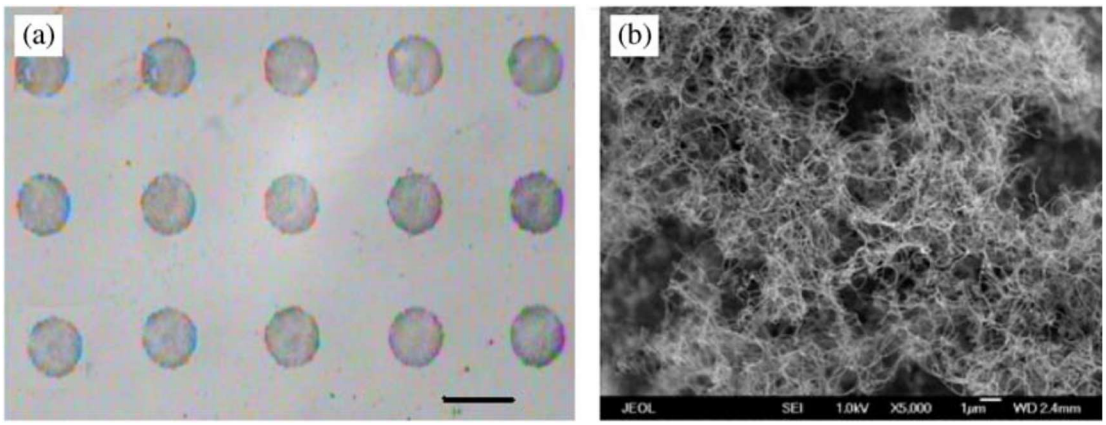

Figure 5: Optical image islands of carbon nanotubes (a). SEM image of island coated by nanotubes (b).[28]

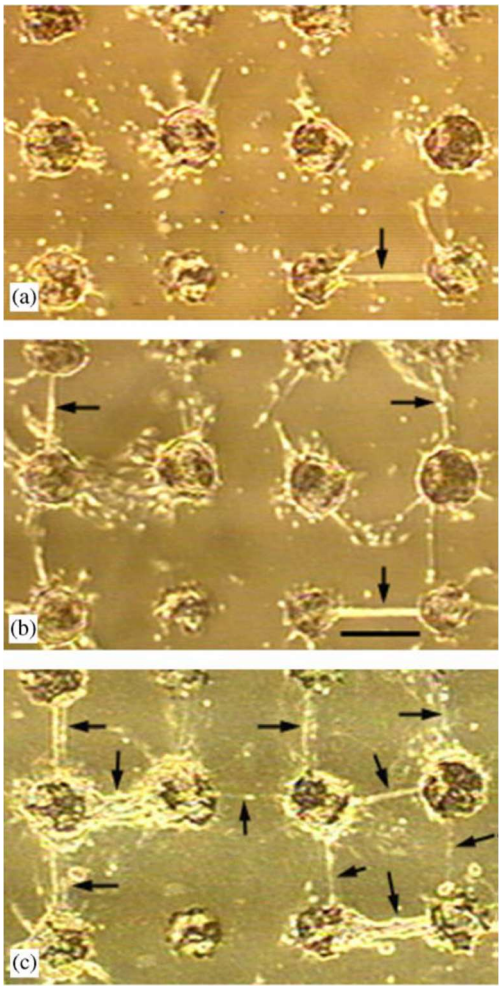

Figure 6: Inverted microscope images of on carbon nanotube islands organized neuronal system. Cluster formations were studied after 96 hours (a), 128 hours (b), and 150 hours (c). With time, the islands became more connected.[28]

In the study of Kwan *et al*, silver nanoparticles sped up the healing process of skin injuries. The presence of silver nanoparticles accelerates the process of turning fibroblasts into myofibroblasts, which causes the injury to heal faster. The healed skin using silver nanoparticles accomplished better results of tensile tests than the skin, which was not treated.[29] Good conductive properties were observed in nanoparticles of gold, cadmium selenide, mercuric selenide, zinc oxide, or zinc sulfide.[23] Heat conductivity of gold nanoparticles has been used for treating cancer. Injected gold nanoparticles passively localize the tumor. Using near-infrared light or radio waves as an excitation source together with the conductive ability of gold nanoparticles increases the temperature in the close surrounding of gold nanoparticles and disrupts membranes of tumor cells.[30] Recently, development in nanotechnology has managed to the investigation of magnetic nanoparticles for materials with magnetothermally-responsive properties. This ability could be employed in delivery and therapeutic systems for cancer treatment as well.[31] Nanoparticles have a huge potential to provide *in vivo* imaging without damaging the cell or tissue. The potential

for bioimaging comes from the luminescent abilities of nanoparticles gained from their low dimensions.[32] Arguably the most important feature of nanoparticles used for tissue regeneration are their antimicrobial properties. Most materials are missing antimicrobial activity, thus being ineffective for longer use in the wound as well as create a potentially suitable environment for pathogens growth.[33]

2.3 Antibacterial Nanoparticles

Antibacterial nanoparticles serve as a novel alternative to traditionally used antibiotics (e.g. penicillin, cephalosporins, sulphonamides) since their effectiveness declined in the past years due to excessive overuse in both human and animal medicine. The overuse leads to the creation of secondary resistant bacteria often referred to as a superbug, which is a big problem in the medical field.[33] The bacteria develop drug resistance by altering their cell structure as a response to stress conditions.[34] The key to acquiring secondary resistance lies in the mechanism of antibacterial effect. The difference between the mechanism of the antibacterial effect of nanoparticles and antibiotics lies in the impact on bacterial cellular structure. Antibiotics usually have a specific effect to one component of bacteria structure. For example, penicillin weakens the bacterial cell wall, and bacteria can adapt to the effect by modifying their cell wall to become more antibiotic-resistant. On the contrary to antibiotics, due to the smaller sizes, nanoparticles affect multiple structural components of bacteria cell at a time. For such an unspecific antibacterial effect, it is harder to adapt. The mechanism of nanoparticle antibacterial activity is based on electrostatic interaction between the nanoparticles and bacteria cell walls. It is followed by breaching the disturbed bacteria cell wall. Nanoparticles and their ions can form free radicals, which induce oxidative stress inside the bacteria cell. This can irreversibly destruct bacteria and cause their death.[35] Nowadays, silver oxide and zinc oxide nanoparticles are considered promising candidates for this application.[34] Another advantage of inorganic antimicrobial nanosized agents is the ability to destroy bacteria without hurting ambient cells.[33] Antibacterial nanoparticles can be applied in many fields. It is commonly used in dentistry as a part of dental fillers, face creams, as well as in drinking water and wastewater treatment. It is widely used in medicine as a part of the wound dressing, to speed up the healing process. It can be found in the form of drug carriers or disinfecting surface coatings. Antibacterial nanoparticles help with food preservation and surface protection.[36]

2.3.1 Traditionally Used Antibacterial Nanoparticles

Many different nanoparticle classes, in terms of chemical composition, can provide antibacterial properties [36]. The most widely used classes of antibacterial nanoparticles are shown in Figure 7.

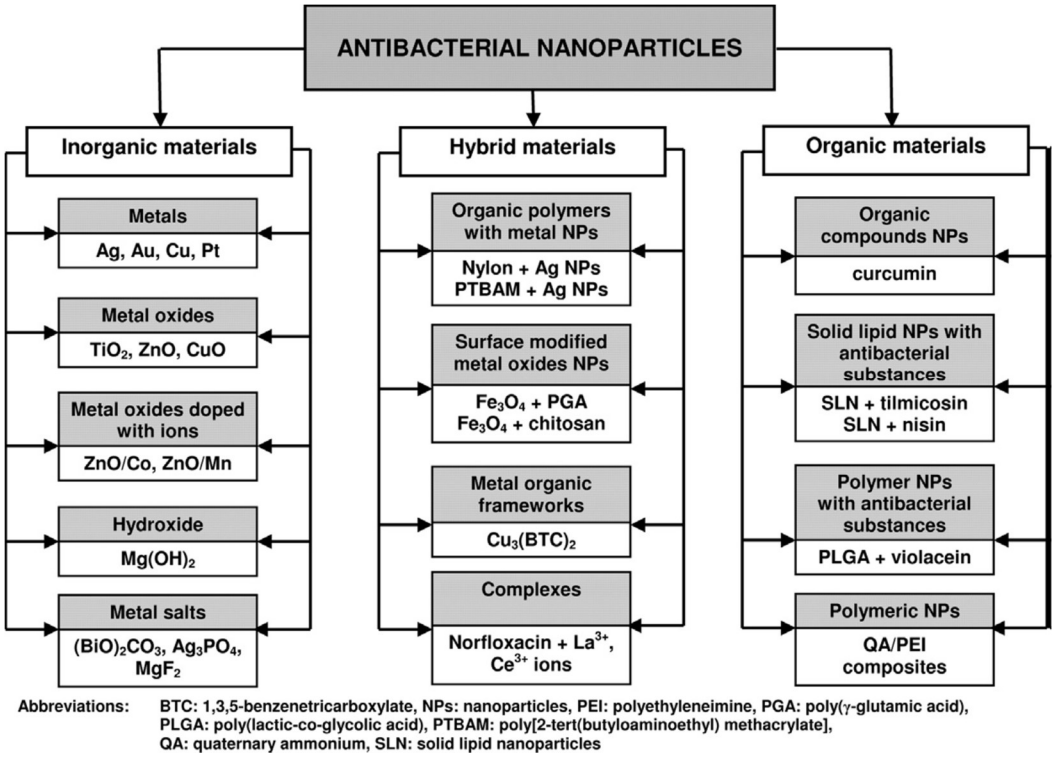

Figure 7: The classification of antibacterial nanoparticles in terms of chemical composition [36].

The first example of commonly utilized antibacterial nanoparticles is copper nanoparticles. Copper is easily approachable metal and it is one of the essential elements in the human body. Toxicity mechanisms of copper nanoparticles towards bacteria cells differ and depend on several factors, such as temperature, pH level, the concentration of nanoparticles, etc. Thanks to electrostatic interactions one of copper nanoparticle toxic mechanisms, starts with the adhesion of nanoparticle on the cell wall of Gram-negative bacteria. The nanoparticle can also affect the structure of proteins in the cell wall, even cause the denaturation process. Alternatively, it can attack parts of the cell, which contain phosphorus or sulphur, such as DNA. Then the bacterial cell lysis follows.[37] The study from 2018, aimed to compare different effects of sodium hydroxide addition on toxicity mechanisms of copper nanoparticles towards Gram-negative *Escherichia coli* and Gram-positive *Staphylococcus aureus.* Nanoparticles were prepared by a facile hydrothermal method while using various concentrations of sodium hydroxide solution. Using a higher concentration of sodium hydroxide brought higher toxicity towards bacteria. Firstly, Cu(II)-peptide complexes are formed, then they attack the negatively charged bacterial cell membranes. It causes the cell wall to wrinkle, which leads to cell fragments and debris formation, as shown in Figure 8.[38]

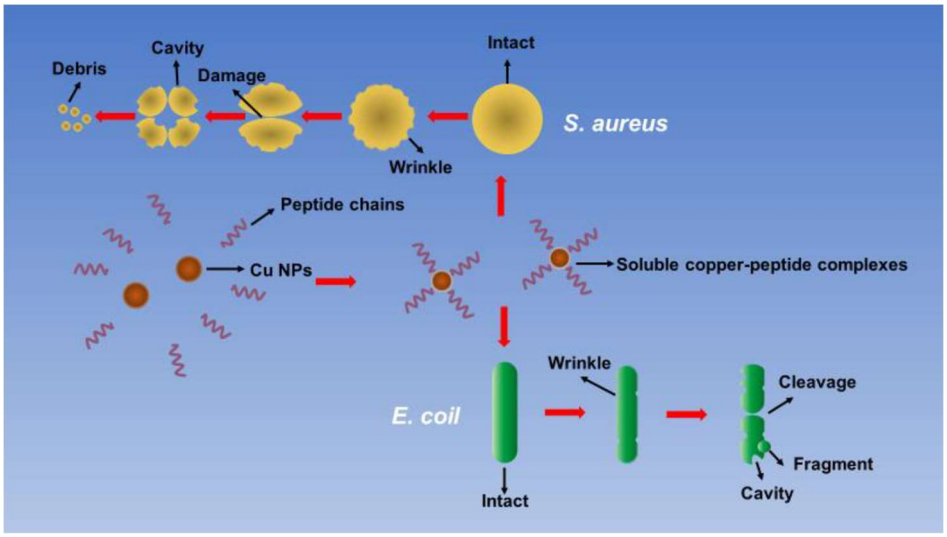

Figure 8: Schematic illustration of antibacterial mechanism of copper nanoparticles to bacteria [38].

Silver nanoparticles are the objects of research of many laboratories, for the sake of their antibacterial properties. Because of this quality, they are widely used in biomedical applications, purification of air and water, food output, textile production, cosmetics, many detergents, and household products.[39] Silver nanoparticles have shown to be effective against many germs such as *Escherichia coli*, *Staphylococcus aureus,* and *Staphylococcus epidermis*, *Bacillus subtilis* among many others.[39],[40]

Gold nanoparticles are utilized in controlled drug delivery, biomedical imaging, and diagnosis, photothermal and gene therapy. In recent years their most studied and most needed possible application is in cancer treatment. The advantage appears from the ability to provide localized, targeted therapy, which has high efficiency, a reduced number of side effects and enhances patient´s life in general.[41] The antibacterial activity of gold nanoparticles is widely utilized. Its ability to restrain the bacterial cell growth and activity has been reported as efficient with both gram-negative and gram-positive bacteria. The apoptosis is caused by nanoparticle adhesion to the cell wall, while inhibiting life-important processes, such as respiration or permeability. The adhesion ability depends on the nanoparticle size, smaller nanoparticles provide bigger surface area and that makes them more effective.[42] The way the gold nanoparticles inhibit the cell growth and cause cell apoptosis can be enhanced by surface modification of the nanoparticles. For example, the nanoparticle capped by polyelectrolyte (PAH) causes a very effective lysis of *Escherichia coli.[43]*

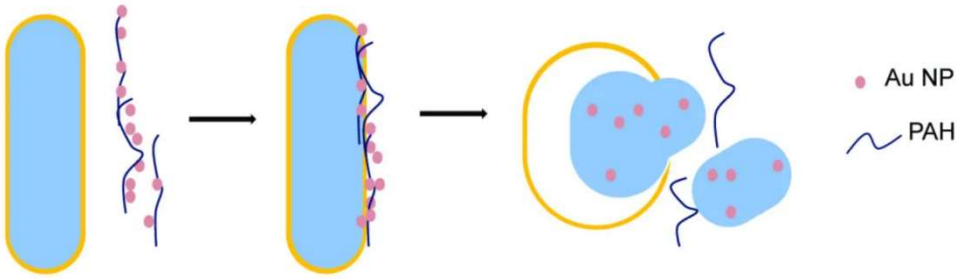

Figure 9: The impact of gold nanoparticles capped by PAH on bacterial cell [43](modified).

Cytotoxicity assigns to any type of harmful effects to cells, that can be favorable towards germs and cancerous cells as well as disadvantaged if led to damage human cells.[39] Silver nanoparticles have shown toxicity to higher organisms, in many previous studies.[44] It was proven that silver nanoparticles can induce inflammation in the lungs of the examined rats.[45],[39] Silver nanoparticles decrease mitochondrial function and boost membrane leakage of mouse spermatogonial stem cells as well.[46]

2.3.2 Biogenic Antibacterial Nanoparticles

Biogenic elements are presented in the living organisms naturally. Thus, the use of biogenic nanoparticles in living organisms can be less invasive, with potential reuse of these elements in metabolic pathways. Overall, biogenic nanoparticles have biodegradable potential and are better accepted by the human body.[47]

MgO nanoparticles fully meet the criteria of being biocompatible, light metal oxide nanoparticles with antimicrobial properties. The MgO nanoparticles can be fully metabolized and reused by the human body. In the study from 2018, different doses of MgO nanoparticles were used against various bacteria, biofilms, and yeasts, to study its antimicrobial activity. The research concluded that, using MgO nanoparticles with rising concentration inhibits the growth of gram-positive bacteria, such as *Staphylococcus epidermidis* or *Staphylococcus aureus.* It becomes lethal for gram-negative bacteria, for example, *Escherichia coli* or *Pseudomonas aeruginosa*. Nevertheless, no growth inhibition or lethal effect towards yeast, such as *Candida albicans*, was observed even when using the highest concentration. The number of viable cells stayed the same. When used against drug-resistant yeast, such as *Candida glabrata,* MgO nanoparticles provided a fungicidal effect.[48]

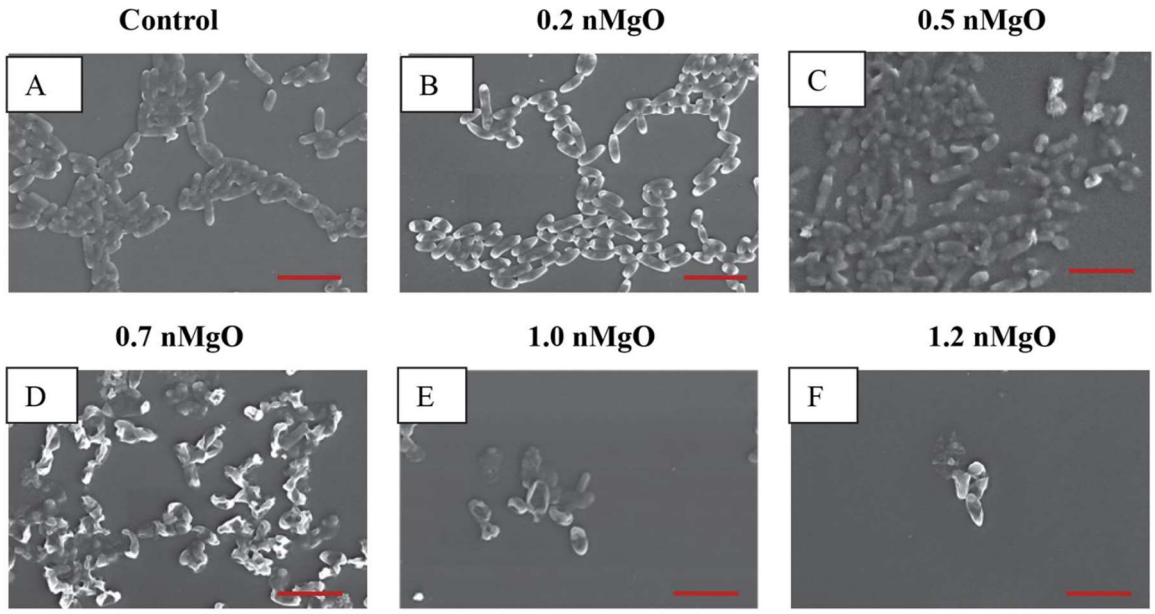

Figure 10: SEM images of Escherichia coli, showing its morphology after cultured with 0-1.2 mg/ml of MgO nanoparticles for 24 hours [48].

ZnO nanoparticles have shown powerful antimicrobial properties against many types of bacteria. The interaction between ZnO nanoparticle and bacterial surface or bacterial core starts the bactericidal process. ZnO nanoparticles have been widely studied for application in various science fields. Owing to their photocatalytic feature, they are used for decreasing water pollution. Seeing that ZnO nanoparticles can absorb UV radiation, they are frequently used as a component in cosmetics, such as day creams and sunscreens. ZnO nanoparticles are highly stable and exhibit implicit photoluminescence features, which are advantageous in bioimaging applications. They are also promising to be biosensors for diabetes, hyperlipaemia, and high cholesterol treatment. Lately, they have been studied mostly for their possible use in cancer treatment. As it is mentioned before, their properties differ from size to size. The same applies to their biodegradable property. ZnO nanoparticle has to be bigger or equal to 100 nm, in size to become to some extent biocompatible.[49] These nanoparticles can be naturally found in human cell proteins and biomolecules [50].

2.4 Selenium Nanoparticles

Selenium as a non-metal element is a very important part of the human diet. It is necessary for healthy life to consume the proper amount of selenium. It is mostly found in proteins.[51] Selenium nanoparticles provide better biocompatibility in comparison to other metal nanoparticles such as gold, silver, and others. Selenium nanoparticles have exhibited anticancerous and antioxidant properties.[52] It was proven that even a really small amount of selenium nanoparticles can decrease the proliferation and increase the possibility of cell death in cancer cells.[52],[53] Selenium is known for having a high level of antibacterial activity, because of this fact its range of application possibilities has rapidly grown in recent years. For example, selenium nanoparticles are featured in antimicrobial coatings for food

wrappers, which serve the purpose of keeping the meal fresh for a longer period. In some cases, selenium nanoparticles were able to destroy microbes locally, without damaging the surrounding tissue.[53],[55] Besides the utilization in tissue engineering and food science, these nanoparticles are used in electronics, for example in photocopiers [56].

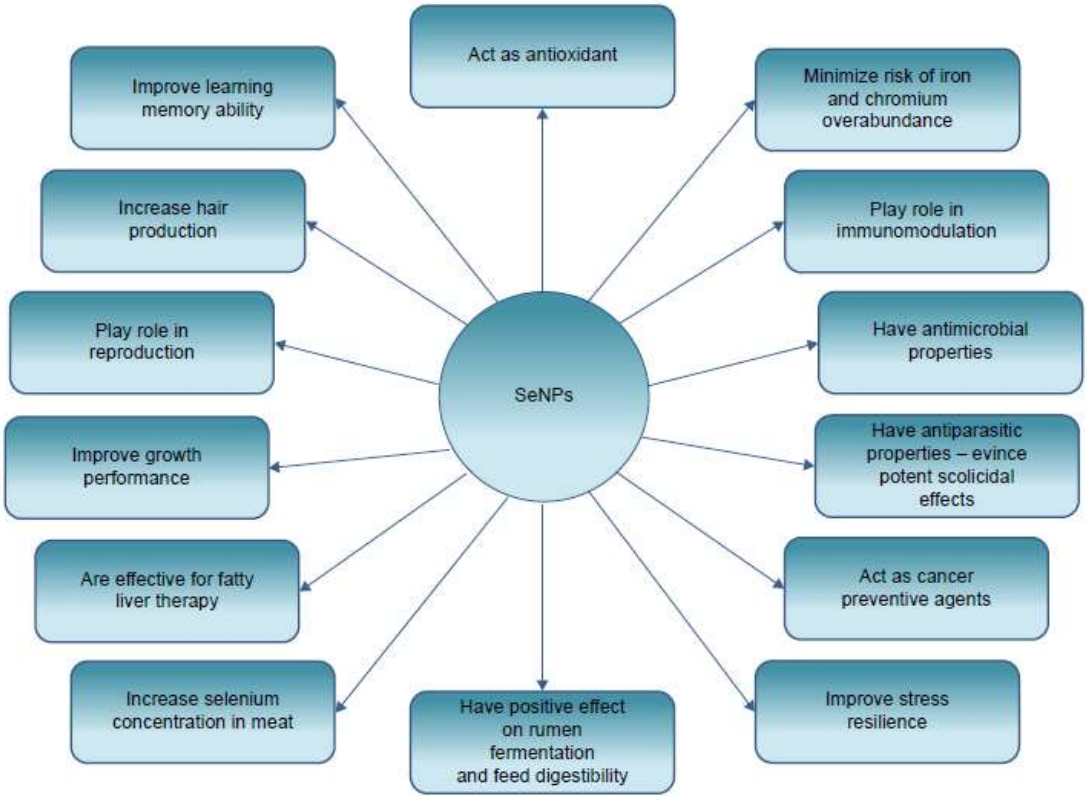

Figure 11: Scheme describing the main effects of selenium nanoparticles [57].

2.4.1 Preparation of Selenium Nanoparticles

There are many ways how to prepare selenium nanoparticles. Commonly a bottom-up approach is used. The process begins with a chemical reduction of selenium salt, for example, selenium tetrachloride, induced by reducing agents, such as ascorbic acid. Besides these, a protecting agent is used to stabilize the final product. Different kinds of protecting agents can be utilized, such as poly (sodium 4-styrene sulfonate). The preparation method usually defines the size and shape of the final nanoparticles.[58] Preparation methods usually differ in kind of precursor, reducing agent or stabilizer, which was used in the process of preparing. The reduction can be provided by chemical reducing agents, such as already mentioned ascorbic acid, or bacterial enzymes. When enzymes or chemicals extracted from plants are used, such as from the leaves of Terminalia arjuna, the production is considered an eco-friendly way. It is proved that smaller sized SeNPs have higher biological activity then bigger sized ones. Because of their biological activity, low toxicity and high biodegradability SeNPs are promising to be used in many applications. Their high biodegradability level allows them to be nutrient to human cells as well as to be an antiproliferative medium for many kinds of tumor cells. There are many possibilities to use SeNPs to destroy tumor cells through endocytosis. Apoptosis, as it

is mentioned before can be accomplished by mitochondrial or DNA damage. Other application use of SeNPs as drug delivery vehicles. In the future, SeNPs can be used as antibiotics because of their low toxicity to human cells and the high ability to damage others. The SeNPs have also shown immunostimulatory effects.[52]

2.4.2 Potential Cytotoxicity of Selenium Nanoparticles

Selenium nanoparticles have shown to be both cytocompatible and cytotoxic. The study describing the anticancerous properties of selenium nanoparticles has not reported cytotoxicity towards normal cells. The cytotoxicity of pure selenium bulk was proven to be much higher, than the cytotoxicity of selenium nanoparticles at the same concentration. In comparison between non-biogenic and biogenic nanoparticles, we can assume that in general, biogenic nanoparticles are manifesting lower toxicity than non-biogenic nanoparticles. To prevent unfavorable cytotoxic effects on human cells, selenium nanoparticles can be stabilized in biopolymers or encapsulated.[53]

2.5 Encapsulation as a Method for Designing Nanoparticles with Specific Parameters

Encapsulation is a method in which the substance is coated with another material. Inside the capsule, the substance is protected against the environment and vice versa. Thus, the encapsulation process is mainly used for lowering the cytotoxicity down or to change the release profile of encapsulate, which is slowed down by the degradation of the capsule. Moreover, the coating material can add additional properties to the substance inside. In the study of Liong et al, the encapsulation of silver nanoparticles inside mesoporous silica nanoparticles led to a slower release of antibacterials silver.[59] The study of Thorat et al have shown, the encapsulation as a method for better target delivery as well as the stability of supramagnetic materials.[60] Another advantage of encapsulated material is its higher cytocompatibility and stability in comparison to not encapsulated material.[61]

2.5.1 Methods of Encapsulation

Encapsulation methods are divided into two main groups, by the type of utilized process. Encapsulation can be either physical or chemical. Physical encapsulation focuses on methods, attainments, and knowledge of physical chemistry. Many concrete techniques are allied to physical encapsulation, for example, adsorption on a seed, in which the encapsulating agent layers are adsorbed on an oppositely charged seed. This method is provided by electrostatic interactions. Other examples of physical encapsulation are heterogeneous polymerization or double emulsion-like process.[62] The second type of encapsulation techniques is chemical encapsulation, such as simple or complex coacervation. A coacervate is a very small droplet, which is fastened by hydrophobic bonds. The coacervation method is based on the partition of hydrocolloids from the emulsion and localization of produced coacervate around the active agent.[63] Layer by layer deposition method is usually used for creating multi-layered shells for encapsulation. It is based on the idea of consecutive layering of encapsulating media on the surface of the encapsulated material. The amount and shape of layers can be controlled,

when using this method.[64] Spray drying is a very low-cost, flexible, and extended encapsulation method. This method is based on inserting the homogenized encapsulating agent into a spray dryer and atomizing it with jet or wheel. Usually, produced spherical particles fall to the ground of drier.[63]

2.6 Dopamine

Dopamine (4-(2-aminoethyl)benzene-1,2-diol) is a biogenic amine, that is a well-known intermediate in the synthesis of norepinephrine and epinephrine [65]. From a chemical structure point of view, dopamine belongs to the group of β-Arylethylamines alongside many other well-known representatives, such as tryptamine, histamine, serotonin, and phenylethylamine. The β-Arylethylamines occur naturally, as a part of the human and animal body nervous system, having the role of neurotransmitters and hormones. Naturally, dopamine and its derivates are formed by α-amino acids decarboxylation. Nevertheless, for the practical use, the dopamine is produced by the reduction of aryl acetonitriles. [66]

2.6.1 Self-polymerization of Dopamine

Polydopamine is produced as a result of dopamine oxidation, which is regarded as relatively quick and simple polymerization. In other words, dopamine can be easily turned into polydopamine, because of its ability to undergo self-assembly polymerization processes.[66] Polydopamine, formed by autoxidation, was firstly described in 1970 as a black material [67].

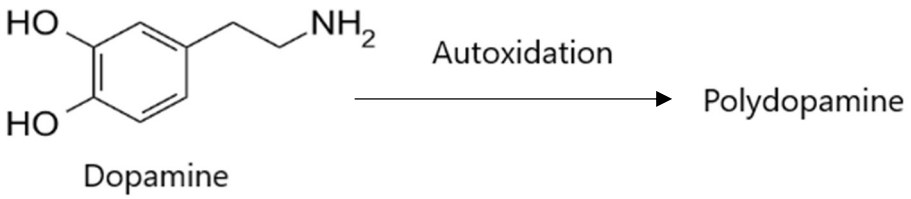

Figure 12: Dopamine autoxidation scheme.

Dissociation of the -OH groups in polydopamine depends on the pH level of the surrounding medium [68]. The effects of different pH levels on the polydopamine molecule are shown in Figure 13.

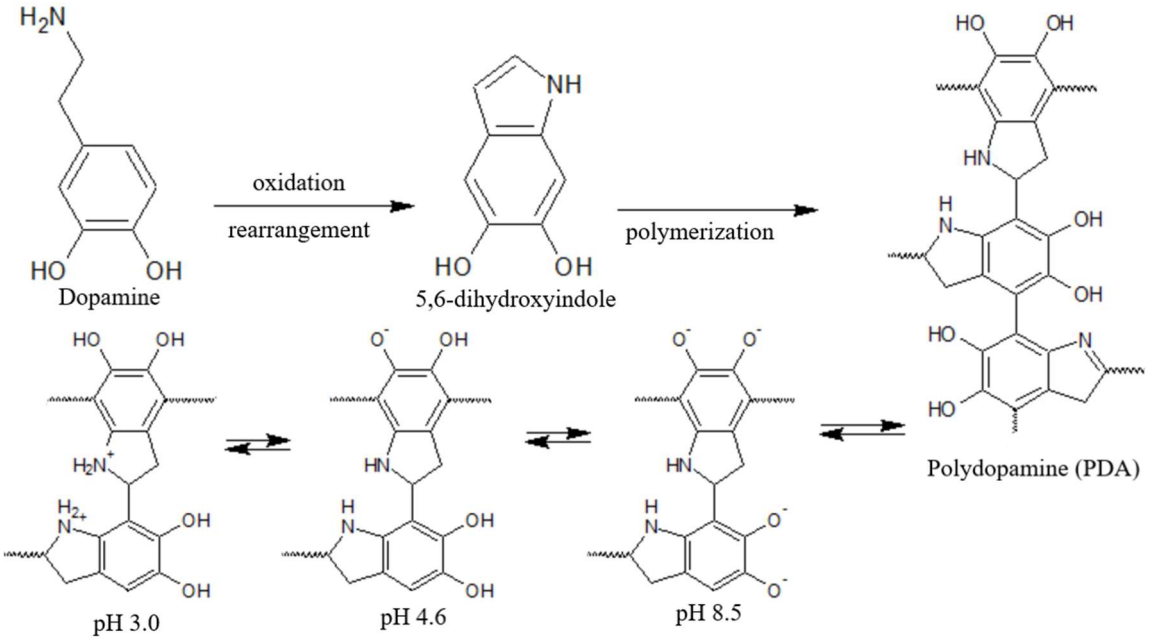

Figure 13: Impact of different pH levels on polydopamine.

The following important study report was released in 2007, containing the discovery of polydopamine ability to adhere to all kinds of surfaces. It can cover huge areas as well as very small ones, such as nano-sized surfaces. It is also able to stick to the surfaces, which are permanently underwater.[69] Since then, polydopamine is treated as a unique material. There have been many successful attempts of its utilization in biomedicine, energy industry, even in the military and other fields. The wide range of its utilization possibilities originates from originates in the variability and simplicity of its production and following use. Nowadays polydopamine is used mainly for material surface modification, which enhances or changes its properties. Many of these properties, which can be found in polydopamine coatings, provide polydopamine coatings a huge advantage over other coating materials, used for surface modification. One of the differences, which allows polydopamine to top other coating methods, is the ability to cover any geometric shape of the surface, wide range of sizes, organic and inorganic surfaces using a simple dip-coating technique or in this case self-assembly coating method. The utilization of polydopamine in biomedicine has generated a big interest among scientists in recent years due to its biocompatibility as a natural in the body occurring substance. This feature can be used in drug coating or this case, encapsulation of particles with antimicrobial effects to control their interactions with cells.[70]

2.6.2 Encapsulation of Nanoparticles in Polydopamine

A study from 2016 aimed to prepare and characterize Fe_3O_4 nanoparticles encapsulated in polydopamine, which works as a photothermal conversion agent. These nanoparticles are magnetic and in combination with 2-phenylethynesulfonamide, considered a possible improvement of photothermal treatment, which is a method of bacterial cell growth interruption. When near-infrared light land on the nanoparticle, the temperature rises and bond strength decreases. Because of that, 2-phenylethynesulfonamide is released. It lowers

the activity of heat shock protein 70 in bacteria, the temperature that can be handled by bacteria is decreased and it ends in bacteria cell death. After the therapy, the magnetic properties of Fe_3O_4 are used to restore nanoparticles. This therapy provides the advantage of reusable material without secondary contamination. To encapsulate, prepared Fe_3O_4 nanoparticles were dispersed in 10 mM Tris-HCl buffer solution, with a pH of 8.5. After that dopamine hydrochloride and $FeCl_3.6H_2O$ were added to the mixture. Within 4 hours of continuous stirring, nanoparticles were successfully encapsulated and loaded with 2-phenylethynesulfonamide.[71]

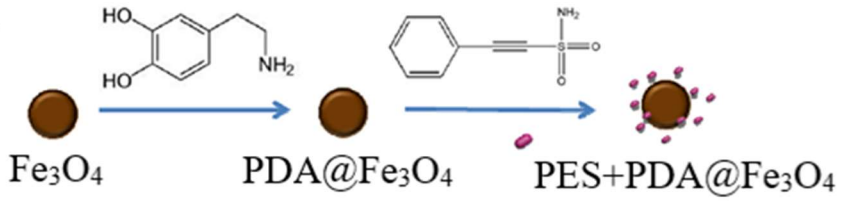

Figure 14: Nanoparticle preparation and encapsulation [71](modified).

The study of Sun *et al*, published in 2017, attempted to use gold nanorods encapsulated in polydopamine as agents with multiple functions for surface-enhanced Raman scattering imaging-guided real-time photothermal cancer treatment method. The process of gold nanorods synthesis was followed by their dispersion in 10 mM Tris-HCl buffer solution, with a pH of 8.5. After that, 1 mg/ml dopamine hydrochloride was added. The reaction continued through the night at a stable temperature of 37 °C, and continuous shaking. Encapsulation was successful and nanorods were ready for further modification, to be suitable for this application. Nanorods maintained surface-enhanced Raman scattering efficiency and were able to undergo photothermal conversion effect. In conclusion, nanorods prepared this way are considered suitable agents for this therapy method.[72]

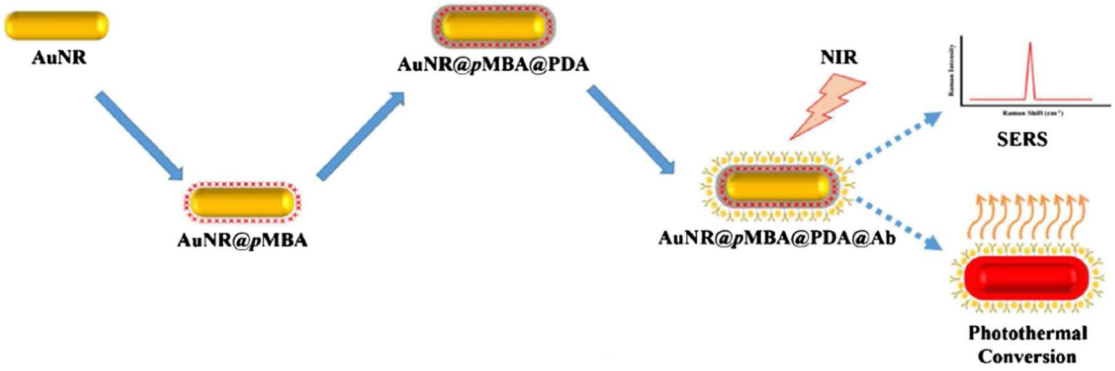

Figure 15: Encapsulation of gold nanorods in polydopamine and its utilization in cancer treatment [72](modified).

Another study from 2018, deals with synthesis, encapsulation, and characterization of fluorescent nanodiamonds encapsulated in polydopamine. Fluorescent nanodiamonds have amazing optical properties that can be utilized in bioimaging. They are also biocompatible,

but easily aggregating in physiological salt solutions. This problem can be easily removed by encapsulation in polydopamine. Nanodiamonds were successfully encapsulated in polydopamine, using buffer solution (pH of 8.5), by oxidation and self-polymerization of dopamine hydrochloride. Originally, nanodiamonds had asymmetrical shapes, sharp edges, and wide range of sizes. When encapsulated, edges of final nanostructures were smooth, absorption abilities increased. The method is described as easily reproducible and robust.[73]

One of the latest studies of Zhu *et al*, published in 2020, deals with nanostructures containing perfluorocarbon encapsulated in polydopamine for possible utilization in ultrasound contrast imaging and photothermal therapy. The first step of the encapsulation process was the mixture of deionized water, ethanol, and ammonia preparation. The mixture was continuously stirred for 30 minutes, then dopamine hydrochloride was added. The mixture was let to undergo the polymerization reaction for 24 hours. Perfluorocarbon was added in a form of nanodroplet and was coated in polydopamine. After encapsulation nanosystems were modified and stabilized by polyethylene glycol. So prepared nanosystems were highly biocompatible, durable, and photothermal conversion efficient. The study confirmed that these nanosystems can be possibly used in ultrasound imaging and photothermal cancer treatment.[74]

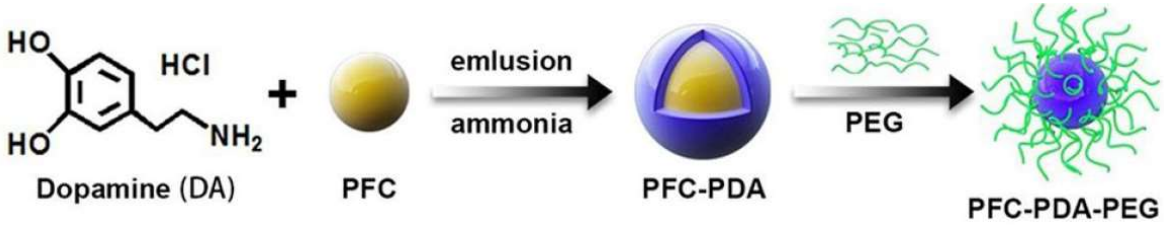

Figure 16: Perfluorocarbon nanodroplets encapsulated in polydopamine, stabilized by polyethylene glycol [74](modified).

3 GOAL OF THE WORK

The goal of this work is to prepare stable antibacterial selenium nanoparticles and find a way to encapsulate them while maintaining their antibacterial activity. It aims to use dopamine's inherent ability to self-polymerize in a basic environment, adhere and cover any kind of surface. Another goal of this thesis is to study the impact of encapsulation to the physical and chemical properties of biogenic selenium nanoparticles.

The experimental work includes followed steps:

- Selenium nanoparticles (SeNPs) synthesis and stabilization via different polymers
- Optimization of SeNPs encapsulation with polydopamine self-assembly
- Chemical structure characterization in terms of ATR-FTIR
- Morphology and SeNPs size characterization using STEM
- Data evaluation and discussion

4 EXPERIMENTAL PART

4.1 Material and equipment

4.1.1 Chemicals

- Ultra-pure water type II according to ISO 3696.
- Dopamine hydrochloride g.r. (Sigma Aldrich, Germany)
- Tris(hydroxyamino)methane g.r. (Sigma Aldrich, German)
- Ethanol 98% g.r. (PENTA, Czech Republic)
- Hydrochloric acid 35% g.r. (lach:ner, Czech Republic)
- Isopropyl alcohol g.r. (PENTA, Czech Republic)
- Selenium tetrachloride g.r. (Sigma Aldrich, Germany)
- Ascorbic acid g.r. (Carl Roth®, Germany)
- Poly (sodium 4-styrenesulfonate) g.r. (Sigma Aldrich, Germany), M_w ~ 70 000
- Sulfuric acid 96% g.r. (PENTA, Czech Republic)
- Oxalic acid dihydrate (PENTA, Czech Republic)
- Potassium permanganate g.r. (PENTA, Czech Republic)
- Ammonium hydroxide 25% g.r. (Carl Roth®, Czech Republic)

4.1.2 Instruments

- pH meter H138 Minilab (Hach®, USA)
- Centrifuge 5804 R (Eppendorf, Germany).
- Magnetic stirrer RET control-visc (IKA®, Germany).
- Vacuum dryer Vacucell 55 comfort (BMM group, Germany).
- Fourier-transformed infrared spectrophotometer Vertex 70/70v (Bruker, United States of America).
- Scanning electron microscope with scanning transmission electron microscopy imaging MIRA3 (Tescan, Czech Republic).
- Analytical balance AV264C (OHAUS, United States of America).
- V-730 UV-Visible/NIR spectrophotometer (JASCO, Germany).

4.2 Preparation of selenium nanoparticles

Two types of selenium nanoparticles, differing in the biopolymer substance that they were anchored in, were used in this work – selenium nanoparticles stabilized by chitosan and selenium nanoparticles stabilized by poly (sodium 4-styrenesulfonate).

4.2.1 Selenium nanoparticles stabilized by chitosan

The pale orange solution of SelenChitosan (SeCh) was synthesized in collaboration with Mendel University. SeCh is a nano-sized system consisting of selenium nanoparticles and chitosan. The preparation process of SeCh nanoparticles was based on the reduction of Na_2SeO_3 using mercaptopropionic acid. The addition of chitosan at the end of the reduction stabilized the reduced selenium (0) in the form of nanoparticles and prevent the nanoparticles against oxidation and agglomeration.

4.2.2 Selenium nanoparticles stabilized by poly (sodium 4-styrenesulfonate)

Selenium nanoparticles were prepared by the bottom-up approach, the chemical reduction of selenium tetrachloride was used according to the previously mentioned study [58]. Selenium tetrachloride was dispersed in ultra-pure water, poly (sodium 4-styrenesulfonate) was added as a protecting agent. The reduction was triggered by ascorbic acid, a reduction agent, and temperature increase to 160 °C.

4.2.3 Washout and re-dispersion of selenium nanoparticles

The washout procedure took place 24 hours after the synthesis of selenium nanoparticles. Firstly, the mixture of the synthesis products was centrifuged (5804 R centrifuge Eppendorf, Germany) at 10 °C. The supernatant was dispersed in about 50 ml of ultrapure water and centrifuged again at 10 °C. The supernatant was collected, and 2 more times dispersed in about 50 ml water and centrifuged at 10 °C. After last centrifugation, the precipitant of washout selenium nanoparticles was collected for further analysis.

4.3 Physicochemical characterization of selenium nanoparticles

4.3.1 Concentration determination of selenium nanoparticles stabilized by chitosan

The concentration of selenium nanoparticles stabilized by chitosan was determined provided by Mendel university.

4.3.2 Concentration determination of selenium nanoparticles stabilized by poly (sodium 4-styrenesulfonate)

The concentration of selenium nanoparticles stabilized by poly (sodium 4-styrenesulfonate) was determined using titration in combination with calibration curve method applied on data acquired from UV/VIS spectroscopy.

The titration was executed according following procedure. Aqueous solution of 0.02 M potassium permanganate solution was utilized as titrant. Prior to the titration, the solution of potassium permanganate was standardized to oxalic acid dihydrate following reaction:

$$5\ (COOH)_2 + 2\ MnO_4^- + 6\ H^+ \rightarrow 10\ CO_2 + 8\ H_2O + 2\ Mn^{2+} \qquad (1)$$

Standardized 0.02 M potassium permanganate oxidized acidified solution of selenium nanoparticles according to the reaction:

$$6\ Se + 10\ KMnO_4 + 5\ H_2SO_4 \rightarrow 6\ HSeO_3 + 10\ MnO_2 + 5\ K_2SO_4 + 2\ H_2O \qquad (2)$$

The solution of acidified selenium nanoparticles was titrated by standardized potassium permanganate solution until a stable pink tint was observed. Titration was repeated three times, afterward exact concentration of selenium nanoparticles was calculated applying stoichiometric coefficients according to equation (2).

Applying the results from the previously mentioned titration, the calibration line for selenium nanoparticles was measured on a UV-VIS spectrometer (V-730 UV-Visible/NIR

spectrophotometer JASCO, Germany). The wavelength interval was set from 800 nm to 250 nm and a halogen lamp was used for these measurements. Prior to the measurement, the cuvette with ultrapure water was measured as a baseline. The stock solution of selenium nanoparticles was diluted to find the nanoparticle ultra-pure water ratio which would provide a stable and well detectable peak. This was followed by the preparation of 5 samples with a known concentration - 150, 125, 100, 75, and 50 nM. The absorptions of these samples were measured. (determined by titration and calculated). The absorbance of these samples was measured at the highest points of their peaks. The calibration line was set, and the calibration equation was calculated in MS Excel.

4.3.3 Morphology and size evaluation

Structure, morphology and size distribution of selenium nanoparticles were determined using scanning electron microscope with scanning transmission electron microscopy imaging (SEM, MIRA3, Tescan, Czech Republic). A small droplet (20 µl) of highly diluted nanoparticles were applied on copper mesh with carbon film (S160, agar scientific, United Kingdom) and were let dried in desiccator overnight. Images were acquired at magnifications ranging from 5 kx – 75 kx using detectors of secondary electrons and transmitted electrons. The images were characterized using software Image J. The sizes of nanoparticles were measured, approximated to circle and their surfaces were calculated.

4.3.4 Chemical structure characterisation

Chemical structure of selenium nanoparticles was evaluated using Fourier-transformed infrared spectrophotometer with attenuated total reflectance equipped with diamond crystal (ATR-FTIR, Vertex 70/70v, Bruker, Germany). Prior to the measurement, nanoparticles were dried out using a vacuum dryer (Vacucell 55 comfort vacuum dryer BMM group, Germany) for 16 hours at 35 °C. Following measurement parameters were set 1.01 hPa pressure level, 4000 – 700 cm^{-1} spectral range, 64 scans with resolution 4 cm^{-1}. Results were exported and evaluated.

4.4 Encapsulation by pH-induced self-polymerization of dopamine

Nanoparticles were encapsulated by self-polymerization of dopamine in the presence of an alkaline medium. More methods and conditions were performed to find the most efficient combination.

4.4.1 Encapsulation method I

In the encapsulation method I selenium nanoparticles and encapsulation are two separated processes. Encapsulation take place after the chemical reduction of selenium salts to selenium nanoparticles. Afterwards, selenium nanoparticles are introduced to basic pH of 0.1 M Tris-HCl (pH 8.5) with dopamine, where dopamine slowly polymerize to polydopamine, which fabricates shell around nanoparticles. The polymerization is driven by the existence of oxygen in surrounding and last 24 hours. The schematic representation of the encapsulation method I is depict in Figure 17.

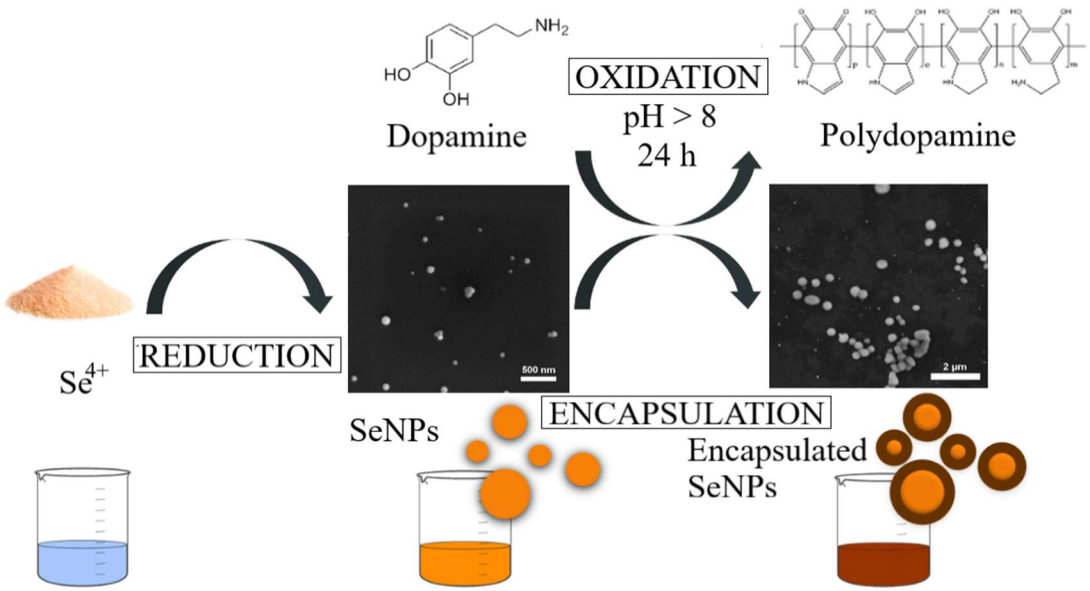

Figure 17: Schematic description of nanoparticle preparation and encapsulation method I

Table 2: Sample preparation description. SeCh – selenium nanoparticles stabilized by chitosan, SePSSS – selenium nanoparticles stabilized by poly (sodium 4-styrenesulfonate).

Sample	Selenium nanoparticles	Selenium nanoparticles [ml]	Ethanol [ml]	ultra-pure water [ml]	Dopamine [mg]	Tris-HCl [ml]
Dopamine polymerization water	-	-	-	35	40	10
SeCh encapsulation method I water	SeCh	15	-	35	40	10
Dopamine polymerization ethanol	-	-	20	15	40	10
SeCh encapsulation method I ethanol	SeCh	15	20	15	40	10
Dopamine polymerization water	-	-	-	35	40	10
SeCh encapsulation method I water	SeCh	15	-	35	40	10
qSeCh encapsulation method I lowered water content	SeCh	15	-	20	40	10
SePSSS encapsulation method I water	SePSSS	20	-	35	40	10
SePSSS encapsulation method I lowered water content	SePSSS	20	-	15	40	10

4.4.2 Encapsulation method II

In the encapsulation method II both processes of nanoparticles synthesis and encapsulation are in progress simultaneously, as it is described in Figure 18. Selenium salts together with dopamine are introduced to basic environment of 0.01 M Tris-HCl (pH 8.5). The oxidative self-polymerization of dopamine to polydopamine creates reductive environment for selenium nanoparticles formation. The polymerization is driven by the existence of oxygen in surrounding and last 24 hours. The schematic representation of the encapsulation method I is depict in Figure 18.

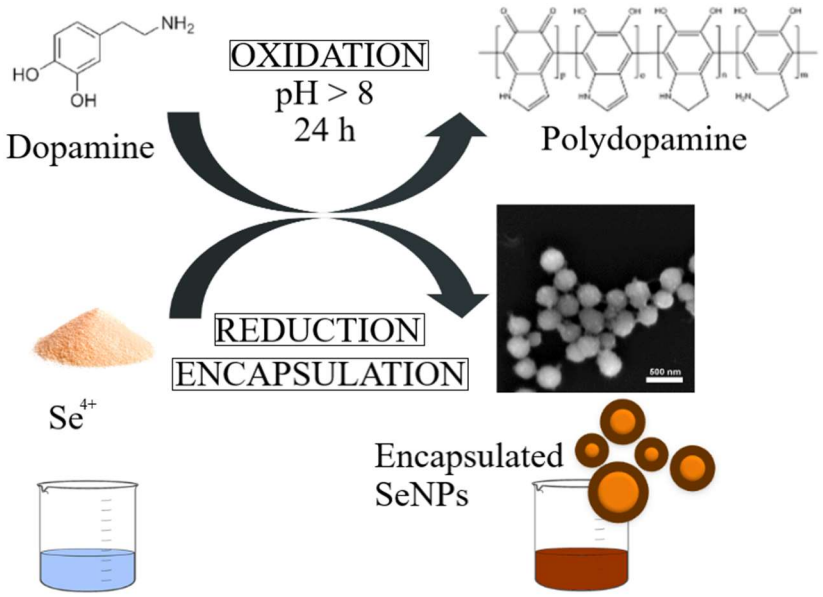

Figure 18: Schematic description of nanoparticle preparation and encapsulation method II.

A sample, which represents the encapsulation method II without using ascorbic acid was prepared by mixing 15 ml of selenium tetrachloride, 40 mg of dopamine, and 75 µl of 25 % ammonium hydroxide. The last sample, which represents the encapsulation method II, while using ascorbic acid was prepared by combining 15 ml selenium tetrachloride with 40 mg of dopamine and 75 µl 25 % ammonium hydroxide. After 24 hours 2.5 ml of 100 mM ascorbic acid solution was added. The mix was stirred under 150 rpm and heated to 160 °C for two minutes just like SePSSS was prepared.

Table 3: Preparation of last two samples.

Sample	Selenium tetrachloride [ml]	Dopamine [mg]	Ammonium hydroxide [µl]	Ascorbic acid [ml]
Encapsulation method II without AA	15	40	75	-
Encapsulation method II with AA	15	40	75	2.5

All samples were centrifugated for 10 minutes at 4200 rpm and washed by ultra-pure water. This process was repeated at least two times in a row.

4.4.3 Washout and re-dispersion of encapsulated selenium nanoparticles

Immediately after finishing the encapsulation in dopamine, the mixture of the synthesis products was centrifuged (5804 R centrifuge Eppendorf, Germany) at 10 °C. The precipitant was dispersed 3 times in about 50 ml of ultrapure water centrifuged at 10 °C. After last centrifugation, the precipitant of washout encapsulated selenium nanoparticles was collected for further analysis.

4.5 Physicochemical characterization of encapsulated selenium nanoparticles

4.5.1 Morphology and size evaluation

Structure, morphology and size distribution of selenium nanoparticles were determined using scanning electron microscope with scanning transmission electron microscopy imaging (SEM, MIRA3, Tescan, Czech Republic). A small droplet (20 µl) of highly diluted nanoparticles were applied on copper mesh with carbon film (S160, agar scientific, United Kingdom) and were let dried in desiccator overnight. Images were acquired at magnifications ranging from 5 kx – 75 kx using detectors of secondary electrons and transmitted electrons. The images were characterized using software Image J. The sizes of nanoparticles were measured, approximated to circle and their surfaces were calculated.

4.5.2 Chemical structure characterization

Chemical structure of selenium nanoparticles was evaluated using Fourier-transformed infrared spectrophotometer with attenuated total reflectance equipped with diamond crystal (ATR-FTIR, Vertex 70/70v, Bruker, Germany). Prior to the measurement, nanoparticles were dried out using a vacuum dryer (Vacucell 55 comfort vacuum dryer BMM group, Germany) for 16 hours at 35 °C. Following measurement parameters were set 1.01 hPa pressure level, 4000 – 700 cm^{-1} spectral range, 64 scans with resolution 4 cm^{-1}. Results were exported and evaluated.

5 RESULTS AND DISCUSSION

5.1 Characterization of selenium nanoparticles

5.1.1 Concentration determination of selenium nanoparticles stabilized by chitosan

The concentration of selenium nanoparticles stabilized by chitosan was determined at Mendel University in Brno. The exact concentration of nanoparticle solution was 7.9867 mM.[75]

5.1.2 Concentration determination of selenium nanoparticles stabilized by poly (sodium 4-styrenesulfonate)

The concentration of selenium nanoparticles stabilized by poly (sodium 4-styrenesulfonate) was determined by titration using a standardized potassium permanganate solution. Because the concentration of selenium nanoparticles was low and the small volume of $KMnO_4$ was needed, the titration solution was diluted in a 1:9 ratio with ultra-pure water, to achieve more accurate results. The average concentration was determined to 0.54186 mM, according to Table 4.

Table 4: Results of titration using $KMnO_4$.

	Volume of $KMnO_4$ used for titration [ml]	Concentration of selenium nanoparticles [μM]
1.	2.3	542
2.	2.3	542
3.	2.3	542

Titration is time-consuming technique, which cannot be used effectively for further studies relating to concentration determination of selenium nanoparticles (e.g. release of selenium nanoparticles from disintegrating polydopamine shell). Solution of selenium nanoparticles have characteristic orange tint, that is concentration dependent. Using this knowledge, UV/VIS spectroscopy was chosen to set calibration line for future concentration-related studies. With known concentration of selenium nanoparticles, the calibration line setting was simply done. The calibration line, shown in, was set using these results and the calibration equation was calculated using MS Excel.

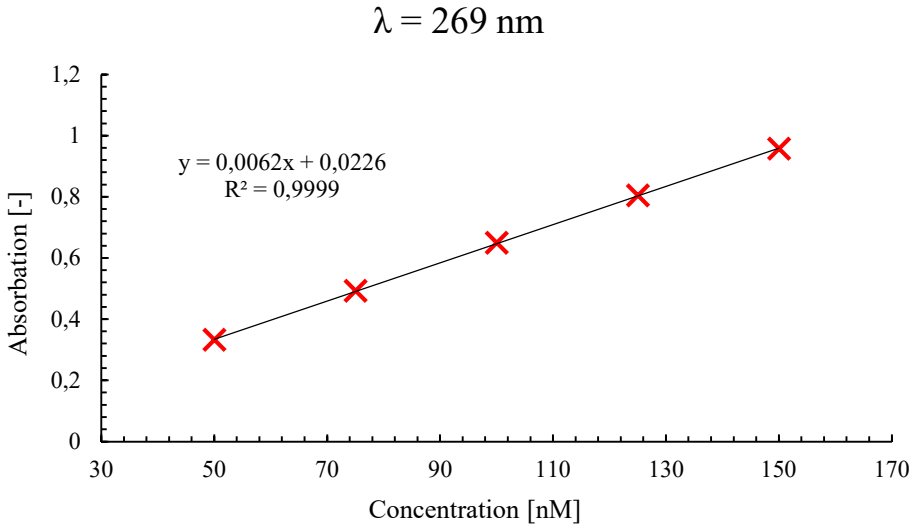

Figure 19: The calibration line for selenium nanoparticles.

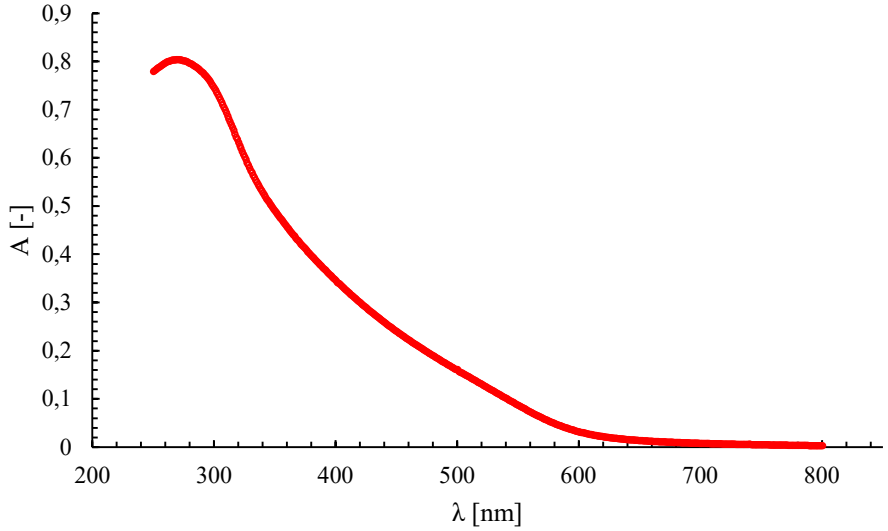

Figure 20: The absorbation spectrum of selenium nanoparticles with concentration 125 nM.

According to Figure 20, selenium nanoparticles reach their maximum absorption around 269 nm. The concentrations of solutions used for calibration line, as well as their maximum absorptions are shown in Table 5.

Table 5: The absorptions of calibration line at 269 nm.

	1.	2.	3.	4.	5.
c [nM]:	150	125	100	75	50
A_{269} [-]:	0.957078	0.80423	0.649418	0.492283	0.33241

5.1.3 Morphology and size evaluation

Both kinds of nanoparticles were studied using scanning electron microscopy equipped with detector for secondary electrons (SE) and detector for transmitted electrons (STEM). Figure 21 shows the SE and STEM image of selenium nanoparticles stabilized in chitosan. Circle-shaped white objects in the left image acquired by SE detector and black objects in the right image quired using STEM detector depicts selenium nanoparticles. The grey-colored clouds localized around the nanoparticles belongs to the chitosan, a polymer used as a stabilizer for the nanoparticles. In Image J software sizes of nanoparticles, without chitosan aggregates, were measured. The size distribution analysis carried out in Image J software evaluated the minimal size of selenium nanoparticles stabilized by chitosan to be 22.41 nm, the largest size to be 150 nm.

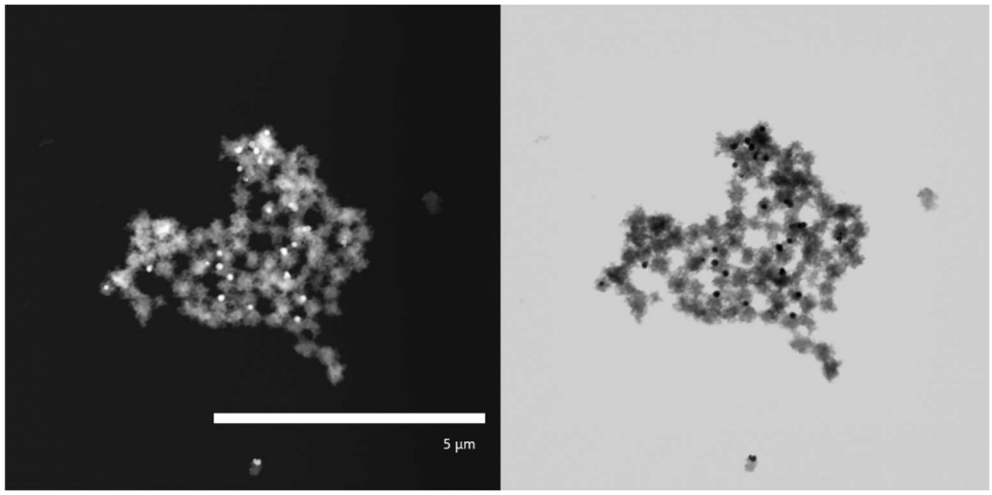

Figure 21: SE and STEM images of selenium nanoparticles stabilized by chitosan.

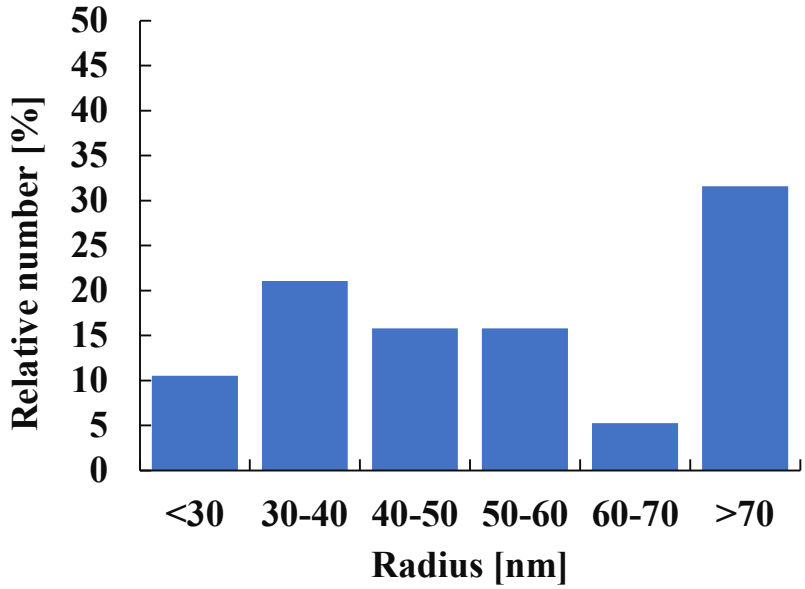

Figure 22: Size distribution of selenium nanoparticles stabilized by chitosan.

Contrary to the selenium nanoparticles stabilized by chitosan, which were prepared by standardized method provided by Mendel University, the selenium nanoparticles stabilized by (sodium 4-styrenesulfonate) were firstly prepared just for the purposes to this thesis. Due to this, the synthesis of the nanoparticles was non-optimized and supernatant and precipitate of these nanoparticles were studied separately. Captured images depict the nanoparticles separated by first centrifugal cycle. Nanoparticles which were presented in the supernatant, were more regularly dispersed and no clouds were observed according to Figure 23. It is possible to assume that nanoparticles in the supernatant were smaller in average size in comparison to nanoparticles stabilized in chitosan. The shape of nanoparticles in the supernatant was mainly circular, few nanoparticle aggregates were observed. As it is shown in Figure 24, nanoparticles stabilized by poly (sodium 4-styrenesulfonate) were smaller in size, minimal size of nanoparticles in the supernatant was 10.5 nm and the largest was 97.5 nm.

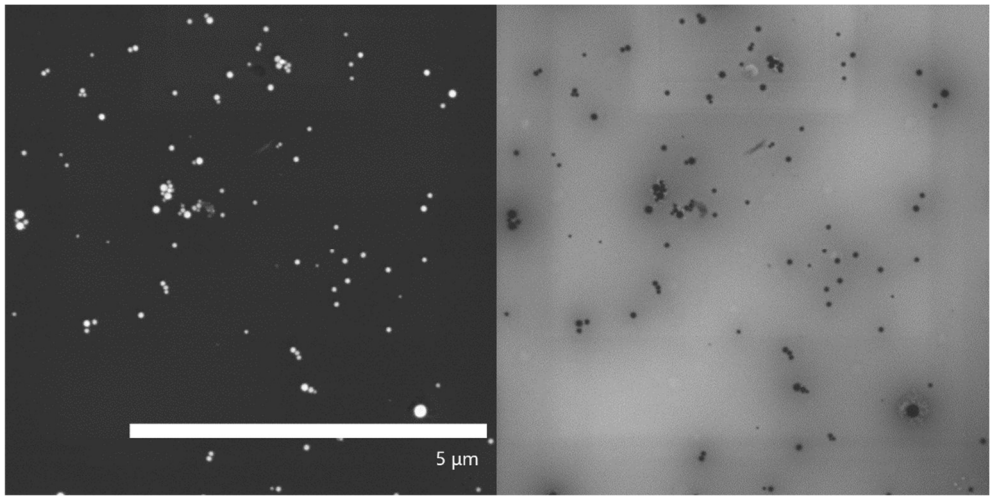

Figure 23: SE and STEM images of selenium nanoparticles stabilized by poly (sodium 4-styrenesulfonate) supernatant.

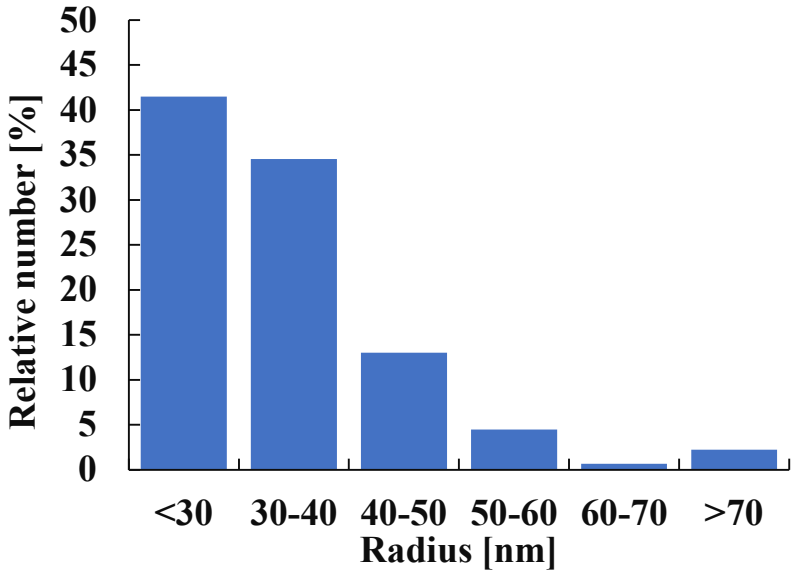

Figure 24: Size distribution of selenium nanoparticles stabilized in poly (sodium 4-styrenesulfonate) supernatant.

The precipitate of selenium nanoparticles stabilized by poly (sodium 4-styrenesulfonate) did not contain protecting agent clouds according to Figure 25. Aggregates in precipitate were more common and larger in comparison to the supernatant. The smallest nanoparticles in precipitate were 13 nm and the biggest was 101 nm. Due to the better dispersion of the selenium nanoparticles dispersed in the supernatant, this portion of selenium nanoparticles was further used in the analysis after proper washout treatment.

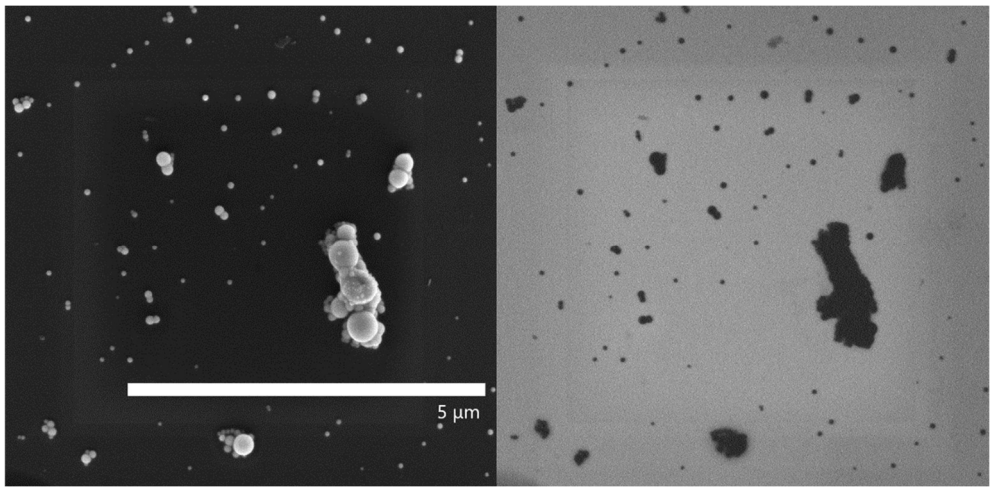

Figure 25: SE and STEM images of selenium nanoparticles stabilized by poly (sodium 4-styrenesulfonate) precipitate.

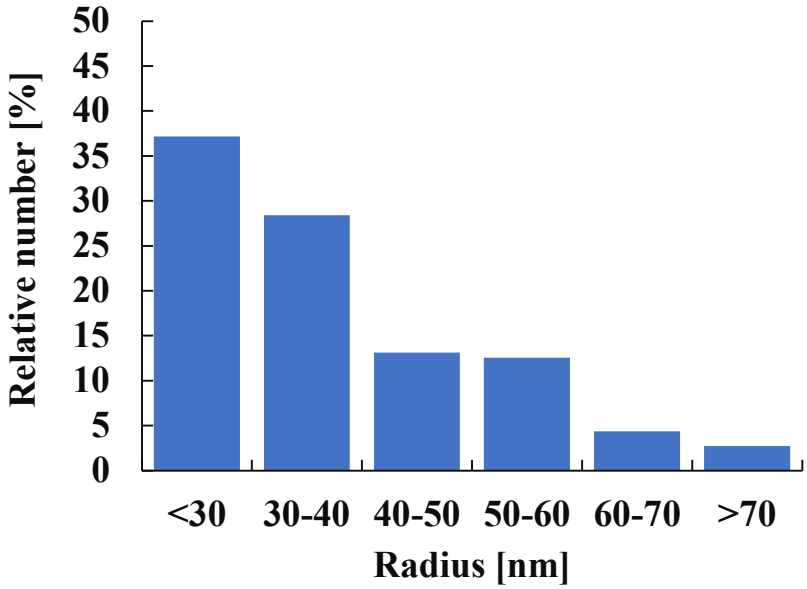

Figure 26: Size distribution of selenium nanoparticles stabilized by poly (sodium 4-styrenesulfonate) precipitate.

Comparing the final histograms of nanoparticle size distribution, it is obvious that Figure 22, which describes the size distribution of selenium nanoparticles stabilized by chitosan, has the biggest average size of nanoparticles. To be precise, the size of up to 32 % of nanoparticles lays within 40-60 nm interval and the same amount, approximately 32 % of nanoparticles is bigger than 70 nm in size. On the other hand, Figure 24 and Figure 26, which represent the size distribution of selenium nanoparticles stabilized by poly (sodium 4-styrenesulfonate), show a much smaller average size of nanoparticles. In both graphs, the mainly represented nanoparticles are 30 nm and smaller. According to Figure 24, more than 41 % of all nanoparticles contained in the supernatant is smaller than 30 nm and 2.24 % is bigger than 70 nm. Precipitate described by Figure 26, contains approximately 37 % of nanoparticles smaller than 30 nm and 2.73 % of all nanoparticles in the precipitate is bigger than 70 nm. The most convenient selenium nanoparticles for our application, seem to be the supernatant of selenium nanoparticles stabilized in poly (sodium 4-styrenesulfonate). It contains no clouds, made from protecting agent, that could possibly inhibit the encapsulation, and fewer aggregates are formed. Also, the average size of nanoparticles is much smaller, approximately 75 % of all nanoparticles is smaller than 40 nm and larger nanoparticles are rarely represented. Lastly, a boxplot shown in Figure 27, was created using calculated data of nanoparticle surfaces in MS Excel. This boxplot was made in order to compare the size distribution among all nanoparticles utilized in the thesis.

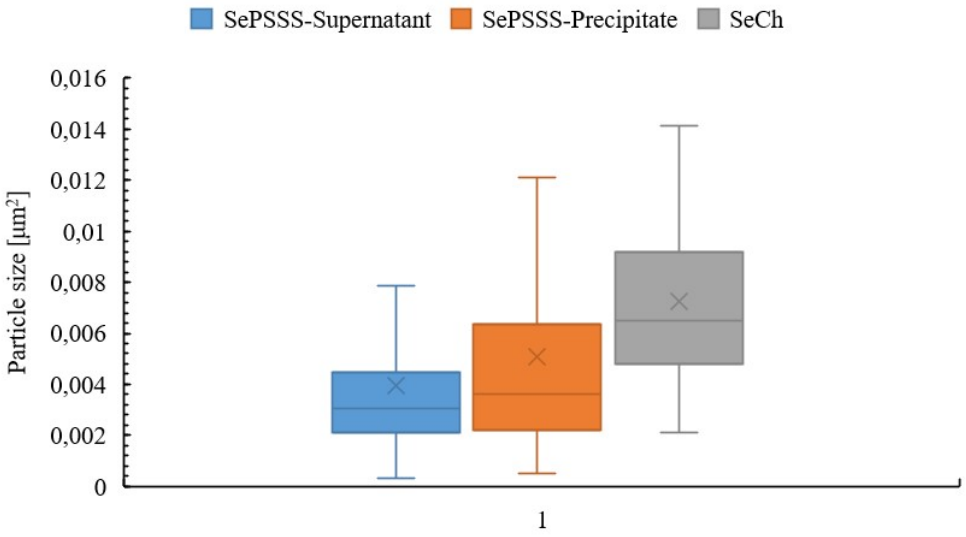

Figure 27: The boxplot representing calculated particle sizes of selenium nanoparticles stabilized by PSSS in supernatant, precipitate, and selenium nanoparticles stabilized by chitosan.

5.1.4 Chemical structure characterization

Method of infrared spectrometry was used mainly to compare differences between the spectrum of selenium nanoparticles with differing protecting agents. The peaks of selenium cannot be observed in FTIR spectra, because peaks representing inorganic matter lay at lower wavenumbers. Because of that, only peaks attributed to chitosan are studied. The FTIR spectra of polymers, by which the selenium nanoparticles are stabilized, were studied. The FTIR spectrum of a vacuum dried selenium nanoparticles stabilized by chitosan is shown in Figure 28. The O-H peak can be observed at 3334 cm^{-1}, a smaller peak at 2914 cm^{-1} represents the C-H group. The highest peak of the spectrum belongs to the N-H group and is located at 1564 cm^{-1}. Last two important peeks are the C-N peak at 1405 cm^{-1} and the peak of the C-O group at 1068 cm^{-1}.

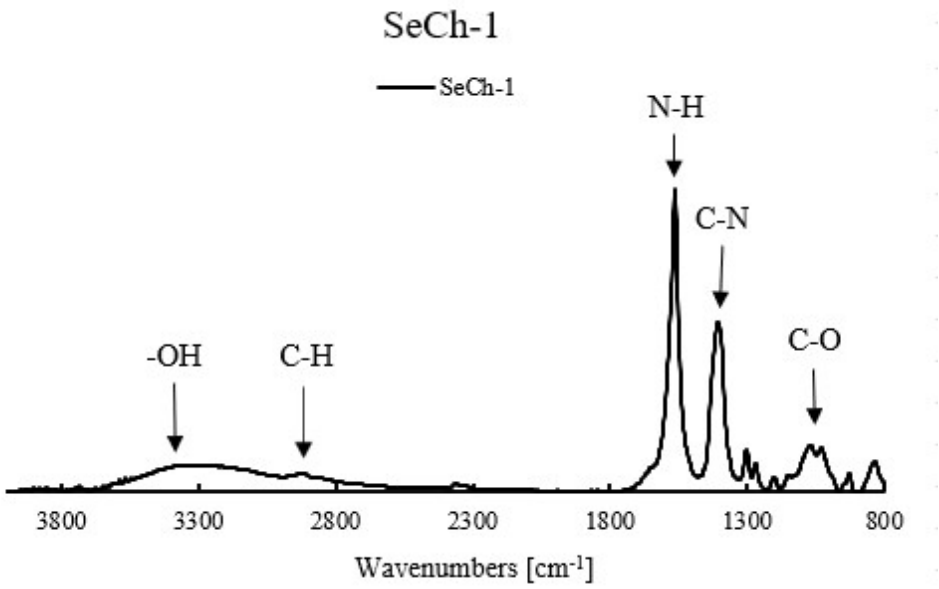

Figure 28: FTIR spectrum of selenium nanoparticles stabilized by chitosan.

The FTIR spectrum of selenium nanoparticles stabilized by poly (sodium 4-styrenesulfonate) is shown in Figure 29. The peaks of selenium are not shown in the FTIR spectrum, because the peaks of inorganic matter are visible at much lower wavenumbers. In this FTIR spectrum only peaks of poly (sodium 4-styrenesulfonate) are shown. The -OH peak lays at 3367 cm^{-1} and is followed by the C-H peak at 2958 cm^{-1}. Stretching vibrations of the C=C group can be observed at 1741 cm^{-1}. The highest peak of this spectrum lays at 1081 cm^{-1} and represents the presence of the S=O group.

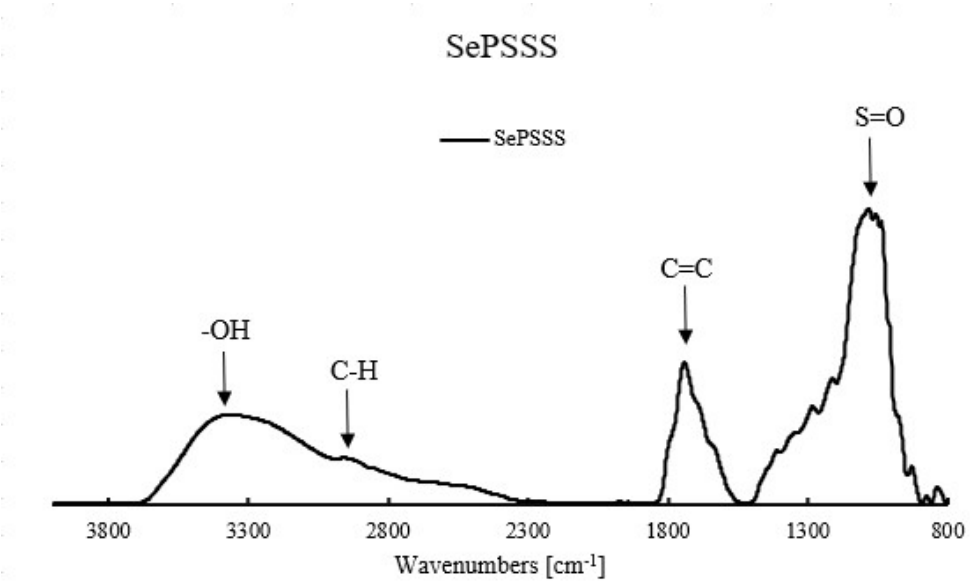

Figure 29: FTIR spectrum of selenium nanoparticles stabilized by poly (sodium 4-styrenesulfonate).

5.2 Encapsulation by pH-induced self-polymerization of dopamine

The polymerization of dopamine in basic solution of basic (pH 8.5) 0.01M Tris-HCl buffer is followed by colour-change. At the beginning of the polymerization all the samples were clear in colour or clear with orange tint, caused by the presence of pale orange selenium nanoparticles in the solution. Examples of original sample colour are shown in Figure 30.

Figure 30: Samples prepared to undergo the polymerization, on the left side sample without selenium nanoparticles present, on the right side samples containing selenium nanoparticles.

Samples were left to undergo the polymerization reaction, in order to encapsulate, for 24 hours. Samples representing the encapsulation method II underwent nanoparticle synthesis and encapsulation at the same time. Exact colour changes are described in Table 6.

Table 6: Colour changes during encapsulation.

Sample	colour at the begining	final colour after 24 hours
Dopamine polymerization	clear	black
SeCh encapsulation method I	clear with orange tint	black
Dopamine polymerization	clear	brown
SeCh encapsulation method I	clear with orange tint	orange
SeCh encapsulation method I lowered water content	clear with orange tint	orange
SePSSS encapsulation method I	clear with orange tint	black
SePSSS encapsulation method I lowered water content	clear with orange tint	black
Encapsulation method II without AA	clear	black
Encapsulation method II with AA	clear	orange

5.2.1 Morphology and size evaluation

Polydopamine

The sample containing dopamine in aqueous environment, was prepared in order to study dopamine polymerization. In Figure 31 the polydopamine bulks are shown. As can be seen, the interesting property of dopamine polymerization is that even without selenium nanoparticles present in the environment, polydopamine forms capsule-like structures. These images imply possibility of polydopamine to encapsulate nanoparticles.

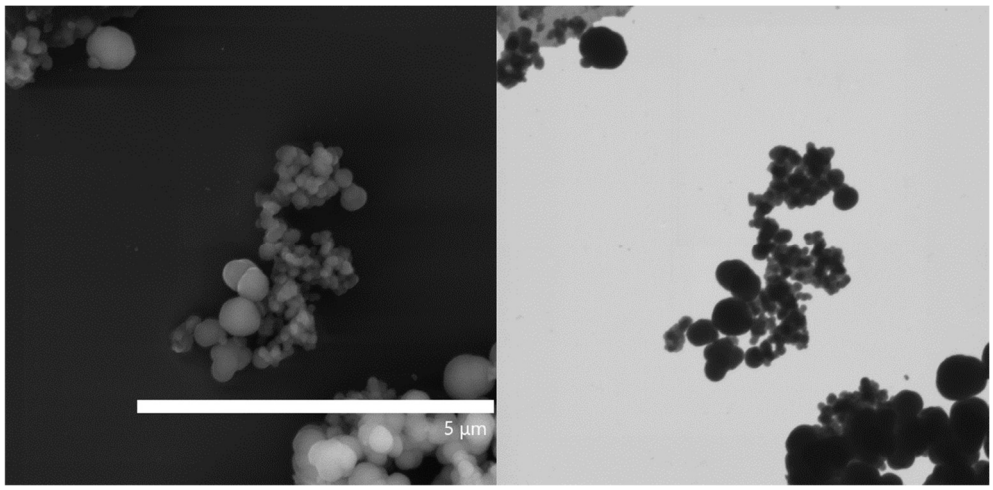

Figure 31:The SE and STEM images of obtained polydopamine.

Encapsulation method I – Selenium nanoparticles stabilized by chitosan

Figure 32 depicts selenium nanoparticles stabilized by chitosan encapsulated by the encapsulation method I procedure. In these images, polymeric aggregates formed around nanoparticles can be observed. This phenomenon is caused by using chitosan as a protecting agent in nanoparticle synthesis. Despite successful polymerization, selenium nanoparticles stabilized by chitosan are not suitable for the encapsulation because nanoparticles are encapsulated in bulks not separately.

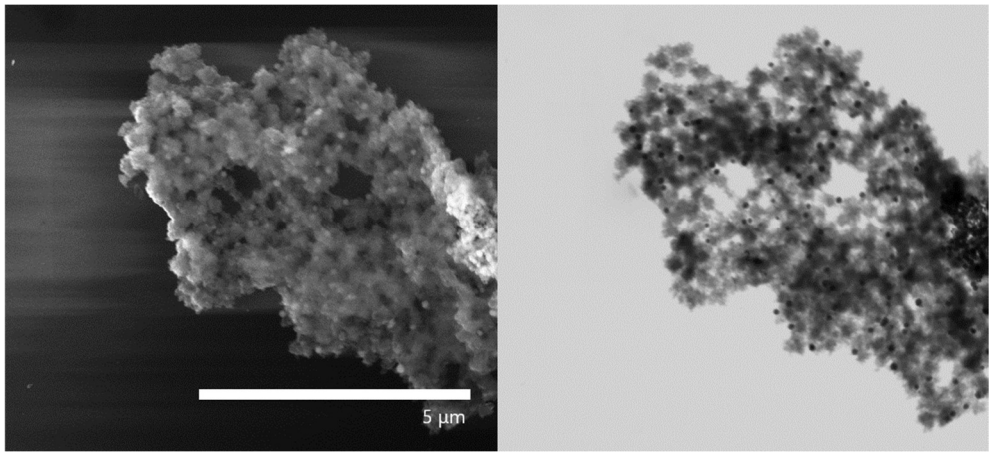

Figure 32:The SE and STEM images of selenium nanoparticles stabilized by chitosan and encapsulated in polydopamine using the encapsulation method I.

Lowering the water content in basic polymerization solutions of 0.01M Tris-HCl did not help formation of polydopamine capsules around selenium nanoparticles stabilized by chitosan. In Figure 45, nanoparticles encapsulated in bulks and polymeric aggregates can be observed. Although these aggregates seem less bulky, still the encapsulation of nanoparticles was not achieved as proposed.

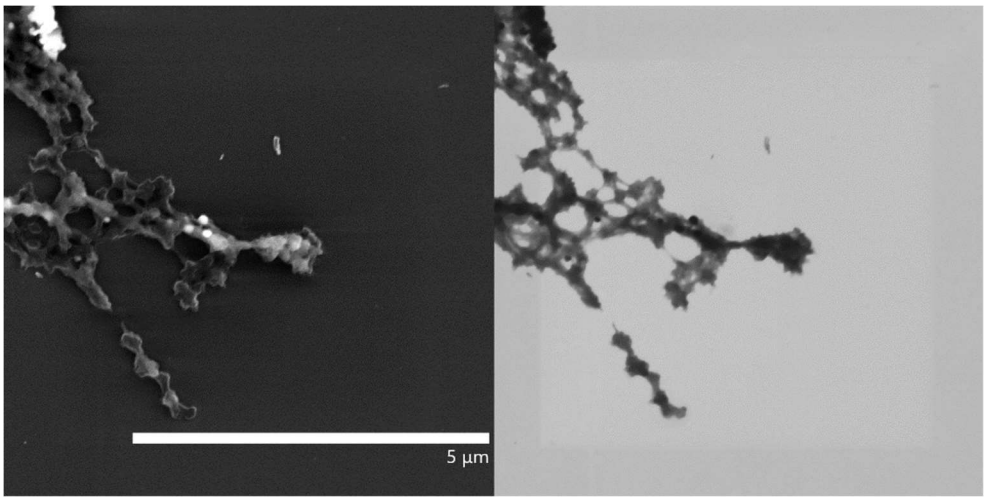

Figure 33:The SE and STEM images of selenium nanoparticles stabilized by chitosan and encapsulated in polydopamine using the encapsulation method I, with lowered water content.

Also, because of these aggregates the sizes of encapsulated nanoparticles cannot be measured properly using Image J program. Because of that, the size distribution histograms are not shown. After these results we were obliged to find other, more suitable selenium nanoparticles for the needs of this type of encapsulation.

Encapsulation method I – Selenium nanoparticles stabilized by poly (sodium 4-styrenesulfonate)

In the preparation processes of following samples, the selenium nanoparticles stabilized in poly (sodium 4-styrenesulfonate) were used, in order to stop polydopamine interactions with protecting agent. Previously this caused production of polymeric aggregates, which did not allow single nanoparticle encapsulation. As it is visible in Figure 34, single nanoparticles seem to be encapsulated. Even though some lighter interaction and aggregation can be observed as well, poly (sodium 4-styrenesulfonate) acted as better protecting polymer permitting the encapsulation of selenium nanoparticles.

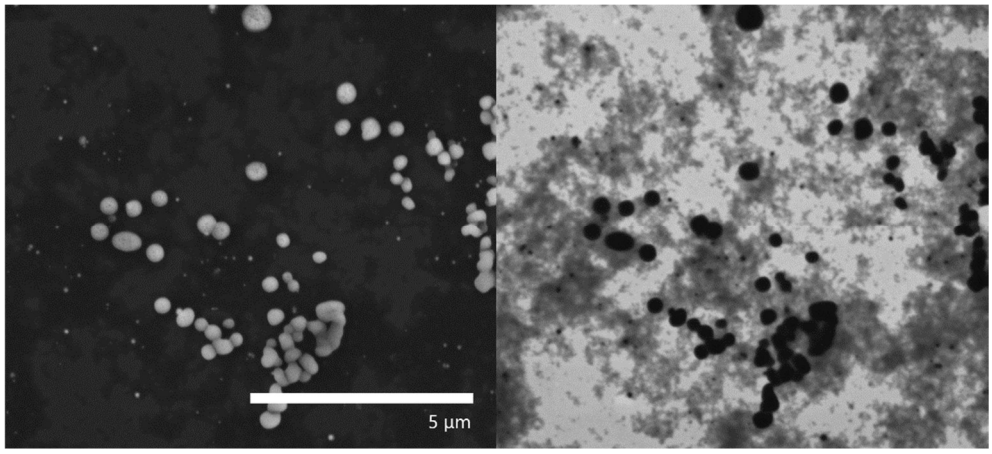

Figure 34: The SE and STEM images of selenium nanoparticles stabilized by poly (sodium 4-styrenesulfonate) and encapsulated in polydopamine using the encapsulation method I.

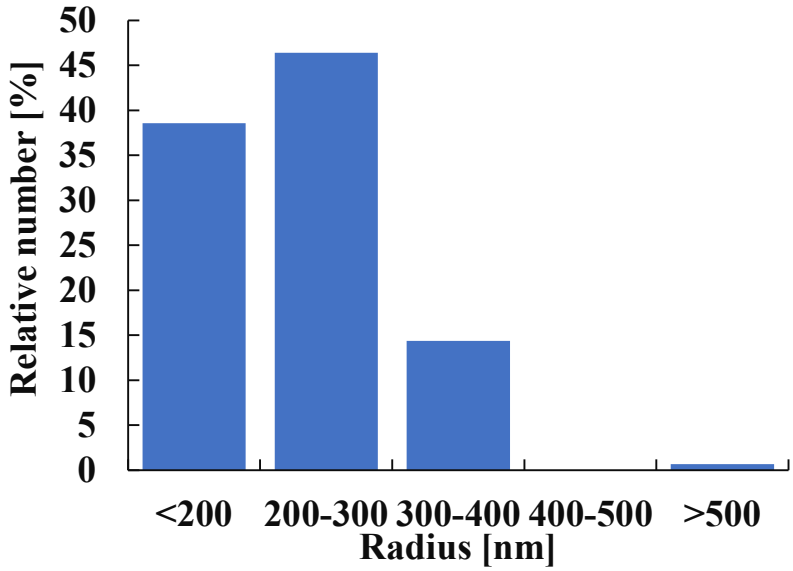

Figure 35: The size distribution of encapsulated selenium nanoparticles stabilized by poly (sodium 4-styrenesulfonate, prepared according to encapsulation method I.

The size distribution of this sample, shown in Figure 35, proves that the radius of encapsulated nanoparticles increased when compared to non-encapsulated nanoparticles. More than 80 % of measured nanoparticles are smaller than 300 nm. Approximately 14 % of measured nanoparticles lay within the interval from 300 to 400 nm and less than 1 % of these nanoparticles are bigger than 500 nm.

It is worth-mentioning that these polydopamine capsules around nanoparticles were relatively unstable. During the scanning of the encapsulated nanoparticles using SEM th particles disintegrated upon longer exposition to 5 kV electron beam. The encapsulated selenium nanoparticles disintegrated also upon time of storage. According to Figure 36, the polymeric shell was not stable after 24 hours in the refrigerator. The polydopamine coating started to disintegrate.

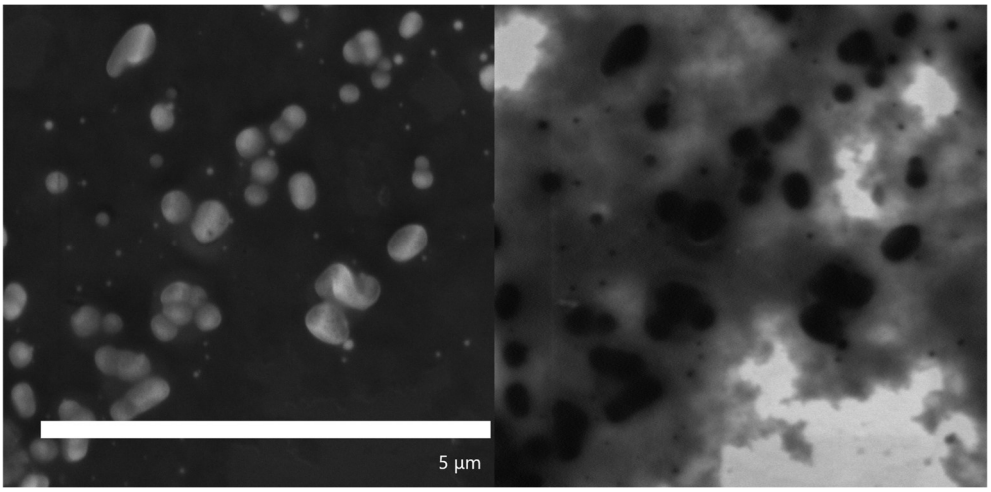

Figure 36: The SE image of encapsulated selenium nanoparticles stabilized by poly (sodium 4-styrenesulfonate), prepared according to encapsulation method I after 24 hours in the refrigerator.

After 48 hours in the refrigerator, the polydopamine shells completely fell apart. Polydopamine then started to form aggregates, as can be observed in Figure 37.

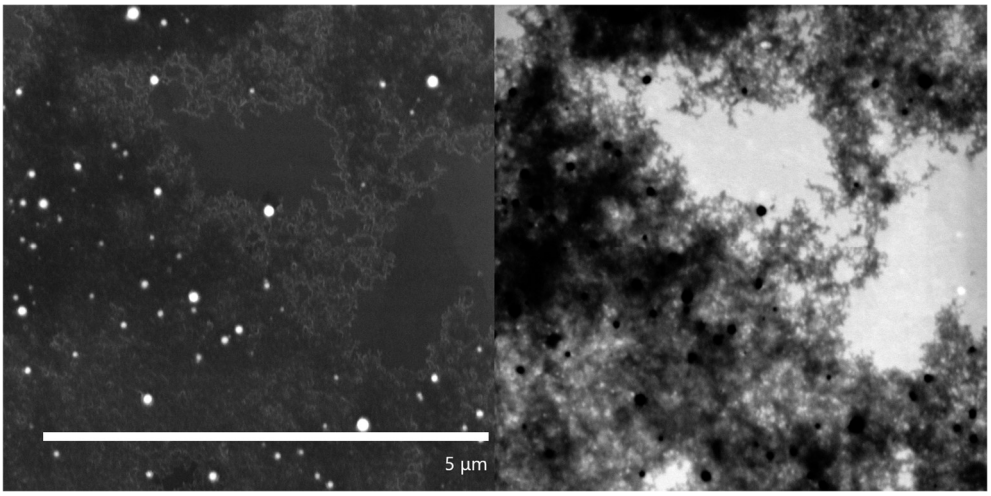

Figure 37: The SE and STEM images of encapsulated selenium nanoparticles stabilized by poly (sodium 4-styrenesulfonate), prepared according to encapsulation method I after 48 hours in the refrigerator.

The influence of lowered water content onto formation of polydopamine capsules was observed as well.

Next sample was prepared similarly to the previous sample, but the content of ultra-pure water was cut down to 15 ml. Comparing SE and STEM images of Figure 34 and Figure 38, the nanoparticles encapsulated in basic solution with lower water not provide separately encapsulated nanoparticles, because of polydopamine, which forms bigger aggregates.

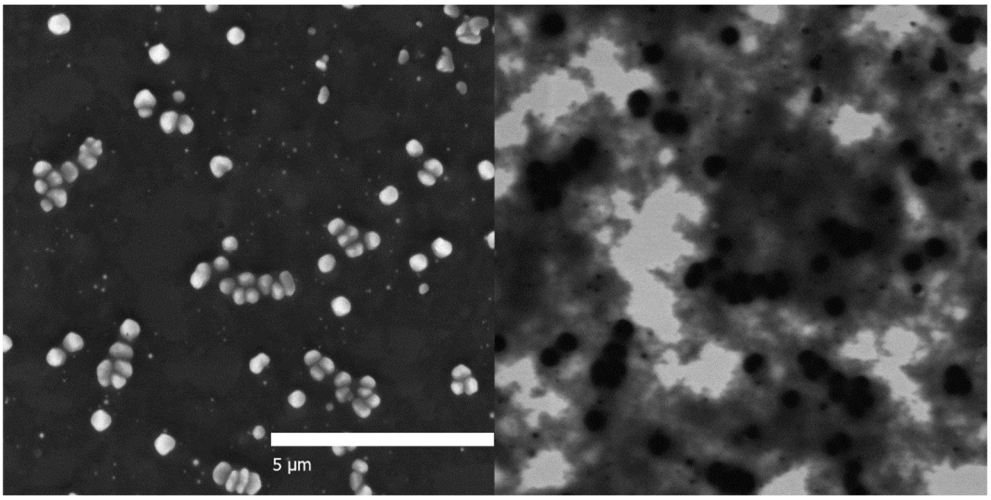

Figure 38: The SE and STEM images of selenium nanoparticles stabilized by poly (sodium 4-styrenesulfonate) and encapsulated in polydopamine using encapsulation method I, with lowered water content.

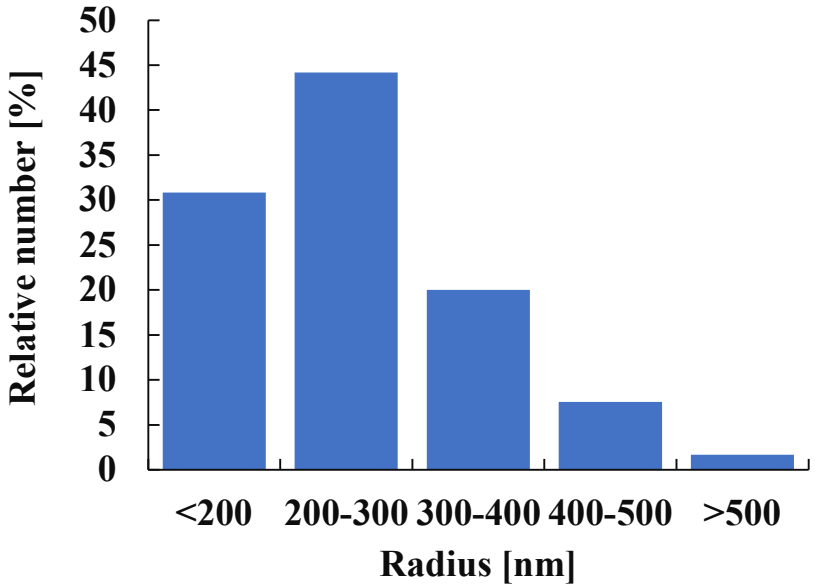

Figure 39: The size distribution of encapsulated selenium nanoparticles stabilized by poly (sodium 4-styrenesulfonate), prepared according to encapsulation method I, with lowered water content.

In Image J measured size distribution of selenium nanoparticles stabilized by poly (sodium 4-styrenesulfonate), prepared according to encapsulation method I, with lowered water content is shown in Figure 39. It is obvious, that most of the nanoparticles lays within 200 to 300 nm interval. Only approximately 2 % of measured nanoparticles is bigger than 500 nm.

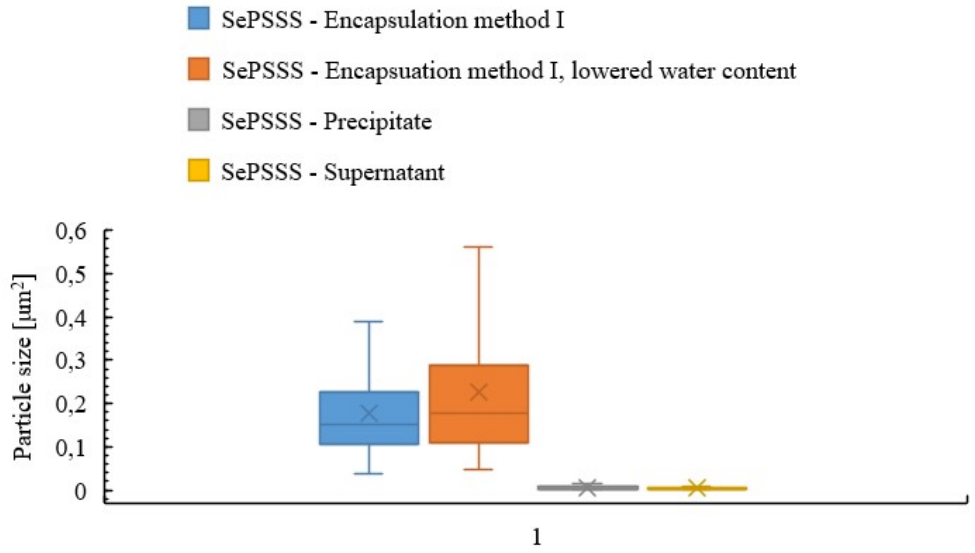

Figure 40: The boxplot containing calculated surfaces of selenium nanoparticles stabilized by PSSS encapsulated in polydopamine using encapsulation method I.

The boxplot representing the calculated particle sizes of selenium nanoparticles stabilized by PSSS encapsulated in polydopamine using encapsulation method I, with and without the lowered water content is shown in Figure 40. It is obvious that nanoparticles, which were prepared with normal water volume came out smaller in size, when compared to nanoparticles prepared with lower water content. As it is obvious from the boxplot encapsulated nanoparticles are much bigger than pure nanoparticles, what is understandable considering the added polydopamine shell.

Encapsulation method II

Principle of the encapsulation method II lies in using reductive environment formed by the oxidative polymerization of dopamine for synthesis of selenium nanoparticles and their encapsulation *in situ*. In this method, polydopamine shell act as stabilizer of fabricated nanoparticles.

It seems that dopamine polymerization was successful. According to Figure 41, the single nanoparticle encapsulation seems to be successful, without the formation of polymeric aggregates. Since no other stabilizer was used for fabricated nanoparticles, polydopamine could cover only the surface of the nanoparticles. Encapsulated nanoparticles seem to be encapsulated symmetrically.

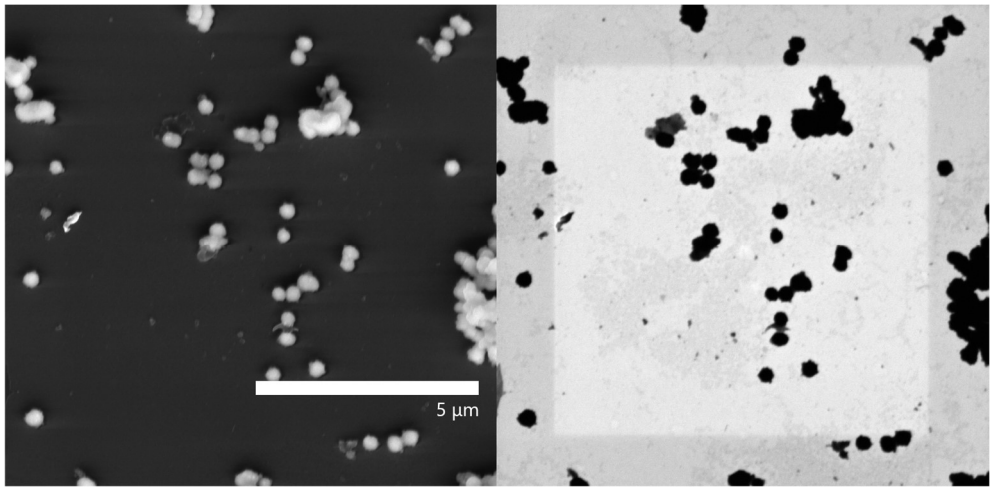

Figure 41: The SE and STEM images of encapsulated selenium nanoparticles prepared by the encapsulation method II, while not using the ascorbic acid.

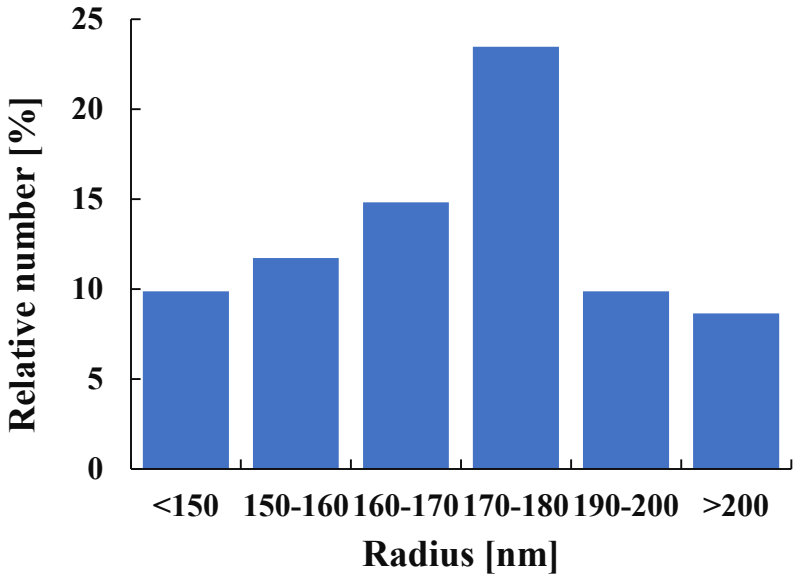

Figure 42: The size distribution of encapsulated selenium nanoparticles prepared by the encapsulation method II, while not using the ascorbic acid.

The size distribution histogram shown in Figure 42 proves that, so prepared encapsulated nanoparticles were much smaller in size, when compared to previously studied encapsulated nanoparticles (SePSSS – Encapsulation method I, etc.). Most of these nanoparticles lays within 170 to 180 nm interval. Up to 10 % of measured nanoparticles are bigger than 200 nm.

The sample was also kept in the refrigerator. As it is shown in Figure 43, encapsulated nanoparticles were stable after 48 hours in the refrigerator.

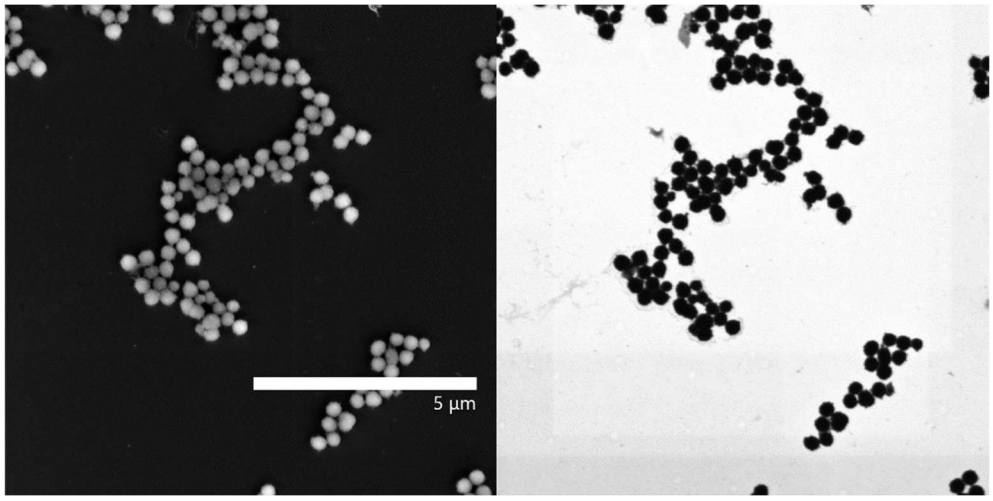

Figure 43: The SE image of PDA_4D sample after 48 hours in refrigerator.

Addition of ascorbic acid, a reductive agent accelerating the fabrication of nanoparticles, into dopamine solution with selenium salt resulted in polydopamine aggregates (Figure 44). These aggregates looked closely alike as polydopamine-coated selenium nanoparticles with chitosan as stabilizer. Nanoparticles seem to be stuck together in bulks, few of them stayed separate. It can be assumed that the ascorbic acid is non-contributory when it comes to successful synthesis and encapsulation of nanoparticles using the encapsulating method II.

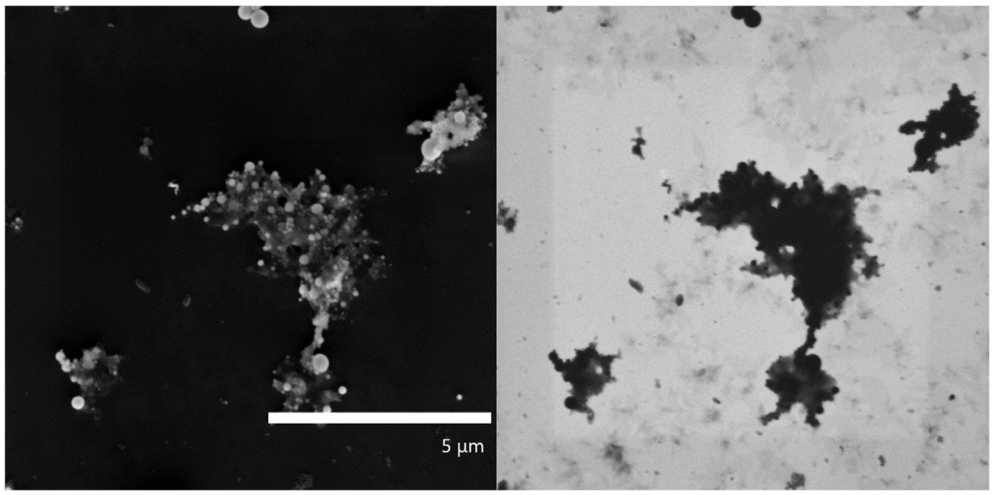

Figure 44: The SE and STEM images of encapsulated selenium nanoparticles prepared by the encapsulation method II, while using the ascorbic acid.

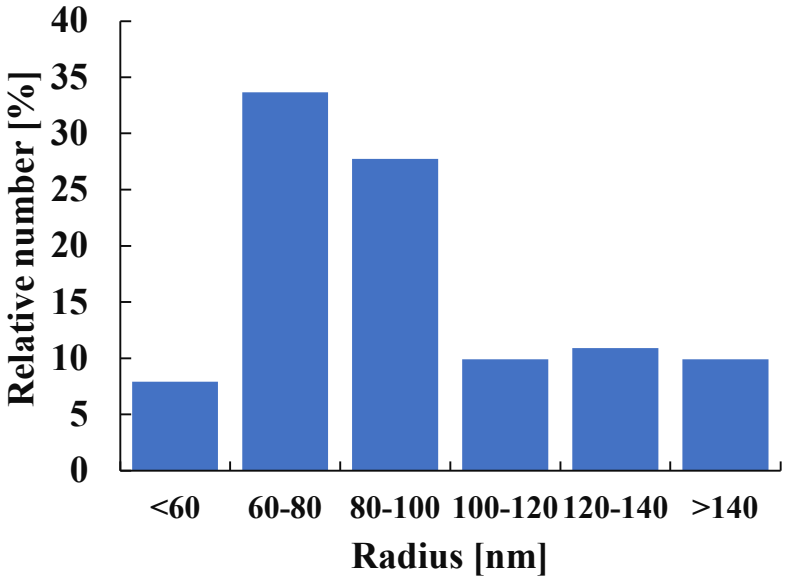

Figure 45: The size distribution histogram of encapsulated selenium nanoparticles prepared by the encapsulation method II, while using ascorbic acid.

As it is obvious from Figure 45, encapsulated selenium nanoparticles prepared according to the encapsulation method II are the smallest in size. Most of measured nanoparticles lay within 60 to 100 nm interval. These might not be the precise measurements of nanoparticles, because this sample tends to form aggregates a lot. The size differences of these samples are shown in Figure 46.

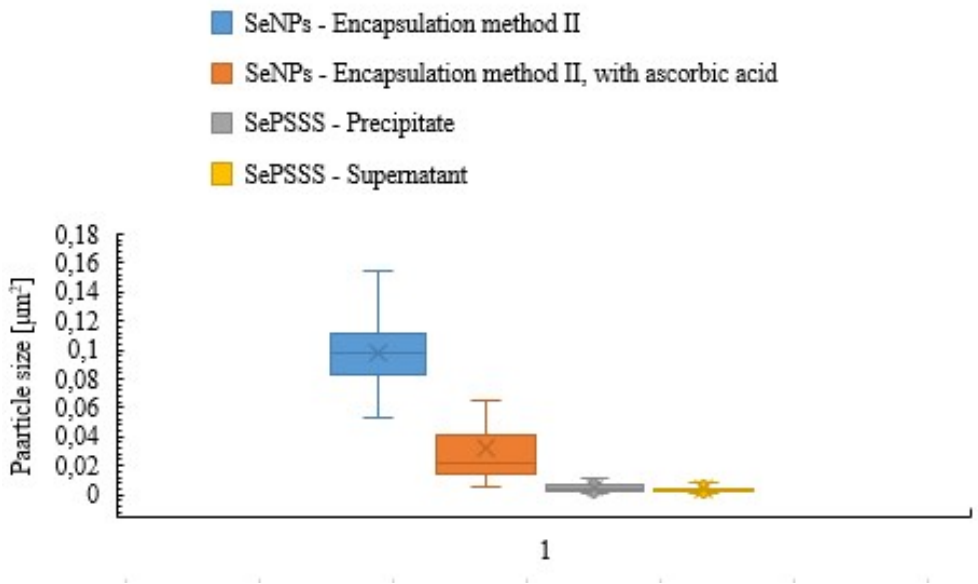

Figure 46: The boxplot of containing calculated surfaces of encapsulated selenium nanoparticles using encapsulation method II.

5.2.2 Chemical structure characterization

Polydopamine

The FTIR spectrum of dopamine and final polydopamine is shown in Figure 47. The -OH peak slightly shifted from 3205 cm^{-1} in the dopamine spectrum to 3194 cm^{-1} in the polydopamine spectrum. The -OH peak of the polydopamine is much stronger and wider. This could be caused by the presence of Tris-HCl in the sample. Stretching vibrations of C=O groups in polydopamine lay at 1581 cm^{-1} and 1281 cm^{-1} and disappeared in the dopamine spectrum. This could be caused by different pH levels. The pH level of polydopamine is higher due to the Tris-HCl addition (pH 8.5), which causes dissociation of the -OH groups in polydopamine. The peaks of C=C groups lay approximately at the same absorption bands, at 1504 cm^{-1} in polydopamine and at 1500 cm^{-1} in dopamine. It signalizes the benzene ring present in the structure. Other characteristic dopamine peaks, such as C-H at 3045 cm^{-1}, and 2958 cm^{-1}, N-H at 1618 cm^{-1}, C-N at 1286 cm^{-1} and C-O at 1176 cm^{-1}, are missing in the polydopamine spectrum. The lack of the C-H group peaks in polydopamine is due to bonds, which are connecting structural subunits in its structure. This could signalize the successful self-polymerization of dopamine.

The main difference, that can be observed when compared to spectra with potentially polymerized dopamine, is that one C-H group is missing from these spectra and the -OH peak is much wider and smoother. Then the presence of the N-H group, which is missing at many other analyzed spectra and C-N group, which is besides the dopamine spectrum observed only in selenium nanoparticles stabilized in the chitosan spectrum. Other sample spectra did not contain this peak. This could be used as a sign of the successful polymerization of dopamine.

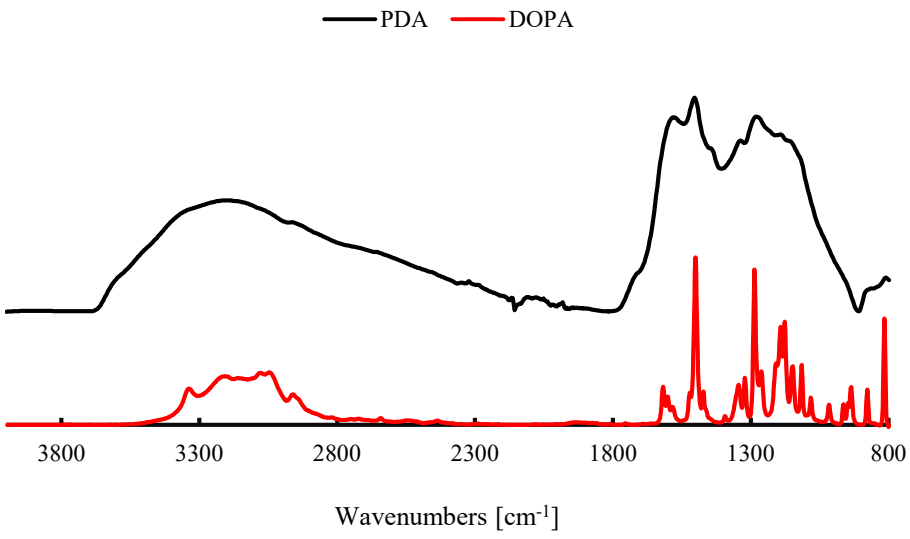

Figure 47: The FTIR spectra of dopamine and polydopamine.

Encapsulation method I – Selenium nanoparticles stabilized by chitosan

The FTIR spectrum of the selenium nanoparticles stabilized by chitosan, encapsulated by the encapsulation method I, is shown in Figure 48. The -OH peak slightly shifted to 3286 cm^{-1} and C-H peaks at 2873 cm^{-1} and at 1415 cm^{-1} arose. The stretching vibrations of C=O peaks shifted to 1635 cm^{-1} and 1377 cm^{-1} and the C=C peak to 1558 cm^{-1}. These shifts are not massive, so similar polydopamine chemical structure is assumed. Differences are in newly accrued peaks such as previously mentioned C-H peaks or for chitosan characteristic CH3-CO- group peaks at 1315 cm^{-1} and 1149 cm^{-1}. The last new peak is for the C-O group, as well as other new peaks it signalizes the presence of selenium nanoparticles stabilized by chitosan. Ultra-pure water content was cut down to 20 ml in next sample, whose spectrum is also shown in Figure 48. It is obvious that lowering the water content during encapsulation process did not provided any significant difference to the FTIR spectrum.

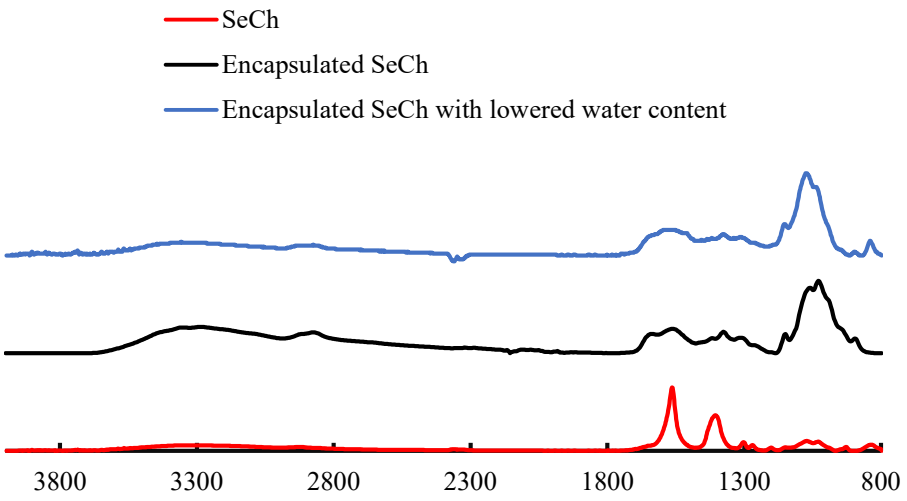

Figure 48: The FTIR spectra of selenium nanoparticles stabilized by chitosan and selenium nanoparticles stabilized by chitosan encapsulated according to encapsulation method I.

Encapsulation method I – Selenium nanoparticles stabilized by poly (sodium 4-styrenesulfonate)

The FTIR spectrum of the sample is shown in Figure 50. The -OH group of encapsulated nanoparticles stabilized by poly (sodium 4-styrenesulfonate) slightly shifted, in comparison with dopamine (3205 cm^{-1}) and pure selenium nanoparticles stabilized by poly (sodium 4-styrenesulfonate) at 3367 cm^{-1} to 3169 cm^{-1}. Stretching vibrations of C-H groups from dopamine (3045 cm^{-1} and 2958 cm^{-1}) and selenium nanoparticles (2958 cm^{-1}) shifted to 2937 cm^{-1} and 835 cm^{-1} in this sample. The first C-H group did not shift much from wavenumbers of C-H peak in dopamine and selenium nanoparticles spectra. It is not quite precise to compare the second C-H group peak of this sample to last peaks of dopamine

or selenium nanoparticle spectrum, because the parts of these peaks lay on the edge of spectra and it is not possible to tell if they have already hit their highest points. The C=C group stretching vibrations shifted from 1500 cm^{-1} in the dopamine spectrum and from 1741 cm^{-1} in the selenium nanoparticle spectrum, to 1599 cm^{-1}, which is a more remarkable shift than in polydopamine spectrum. This group is characteristic for molecules, which contain an aromatic ring. A huge shift can be observed with -NH group, which shifted from 1618 cm^{-1} in dopamine to 1508 cm^{-1} in this sample. This might be caused by cyclization and formation of the upper ring in polydopamine structure. The peaks of the C=O group are present in this spectrum at 1284 cm^{-1} and 1034 cm^{-1}, they are missing in dopamine and selenium nanoparticle spectra. On the other hand, these peaks are present in the polydopamine spectrum. Its presence is considered the result of pH-driven dissociation of -OH groups, which is the side-effect of polymerization. At 1167 cm^{-1}, the peak representing the stretching vibration of the S=O group can be observed. It shifted a little from the wavenumber 1081 cm^{-1} in the selenium nanoparticle spectrum. This peak is characteristic for the samples, in which poly (sodium 4-styrenesulfonate) was used as the protecting agent during nanoparticle synthesis. The C-O peak shifted from 1176 cm^{-1} in the dopamine spectrum to 1034 cm^{-1} in this spectrum. The C-N group peak is missing in this spectrum, this also happened in polydopamine spectrum. These shifts are probably caused by the polymerization process of dopamine described in Figure 49.

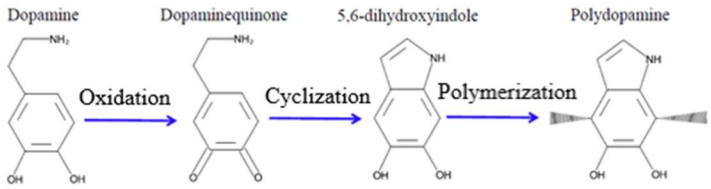

Figure 49: Description of dopamine polymerization process.[76]

According to Figure 50, it seems, that the spectrum of encapsulated selenium nanoparticles stabilized by poly (sodium 4-styrenesulfonate), with lowered water content does not differ much from the spectrum of sample with normal water volume. Many groups have their stretching vibrations at the exact same wavenumbers as in the spectrum of sample with higher water content. The C=C group stayed at 1599 cm^{-1}, N-H group stayed at 1508 cm^{-1} as well, as the S=O group stayed at 1167 cm^{-1}. The second peak of C-O bond stretching did not move and stayed at 1034 cm^{-1}. Also, the second C-H group peak stayed at 835 cm^{-1} as in the spectrum of sample with higher water content. Just a slight decrease in peak intensity can be observed. Besides that, -OH group peak shifted to 3188 cm^{-1}, the first C-H peak shifted to 2933 cm^{-1} and the first C=O peak shifted to 1283 cm^{-1}. In fact, these shifts are so subtle, that it is possible to say that lowering the content of added water did not change the FTIR spectrum at all.

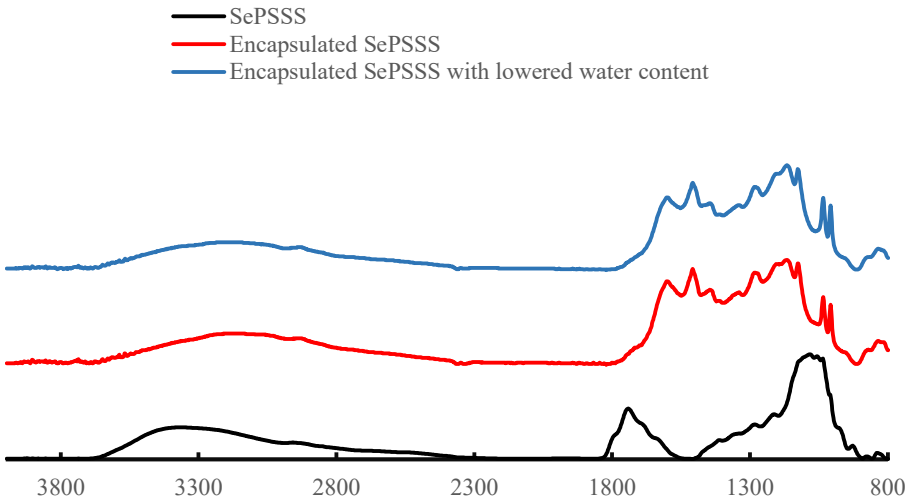

Figure 50: The FTIR spectra of pure selenium nanoparticles stabilized by poly (sodium 4-styrenesulfonate), encapsulated selenium nanoparticles stabilized by poly (sodium 4-styrenesulfonate) with normal water content and encapsulated selenium nanoparticles stabilized by poly (sodium 4-styrenesulfonate) with lowered water content.

Encapsulation method II

These spectra, shown in Figure 51, look unlike any other previously analyzed spectra. The widest peak in the spectrum of sample without ascorbic acid belongs to -OH group, with the highest point at 3246 cm^{-1}, which confirms the presence of hydrogen bonds. Its wavenumber lays somewhere between wavenumbers of -OH group stretching vibration in selenium nanoparticle spectrum and dopamine spectrum. The first C-H group peak lays at 2959 cm^{-1}, which is not considered a massive shift when compared to dopamine (3045 cm^{-1}), selenium nanoparticles stabilized by chitosan (2914 cm^{-1}) spectra. The second C-H peak, which is present in the dopamine and selenium nanoparticles stabilized by poly (sodium 4-styrenesulfonate) spectra, both at 2958 cm^{-1} is missing, what looks to be normal when the dopamine undergoes the polymerization in an aqueous environment, according to analyzed spectra. Next C-H group peak lays at 806 cm^{-1}, but it is not accurate to compare this peak with peaks in other spectra, because their highest points are unknown. Few smaller peaks around 1600 cm^{-1}, signalize the presence of amide bonds. The C=O group and S=O peaks are missing in the spectrum, this is caused by not using the ascorbic acid and poly (sodium 4-styrenesulfonate) in the preparation process. The next peaks in the row are two C-O groups lay at 1186 cm^{-1} and 1043 cm^{-1}. The first C-O peak is not observed in any other sample spectrum, besides the spectrum of dopamine, where it lays at 1176 cm^{-1}. This could signalize some differences in dopamine polymerization.

Next sample was prepared similarly as the previous, the difference was that ascorbic acid was added to this sample. The spectrum shown in Figure 51, looks much different in comparison to sample with ascorbic acid and is more like other encapsulated nanoparticle spectra. The presence of hydrogen bonds in sample with ascorbic acid is confirmed

by the widest, but relatively not extremely high peak at 3230 cm^{-1}. This means that same as in other spectra, the wavenumber lays within the interval from 3367 cm^{-1} to 3205 cm^{-1}, which are the wavenumbers of -OH group both kinds of selenium nanoparticle spectra. The stretching vibrations of the C-H group lay at 2964 cm^{-1} and 806 cm^{-1}, which is quite usual according to other spectra. The C=C group peak is localized at 1605 cm^{-1}, which proves the aromatic ring presence. Stretching of amid group bond is represented by the peak at 1510 cm^{-1}. Because poly (sodium 4-styrenesulfonate) was not added to the preparation solution, the disappearance of sulfonate group stretching as expected. The C=O peak is present at 1302 cm^{-1}, this peak was observed in other samples. These peaks are attributed to pH level change throughout the polymerization of dopamine. Two C-O peaks are present at 1109 cm^{-1} and 1049 cm^{-1}. The C-N peak is not present, which was also observed in other sample spectra.

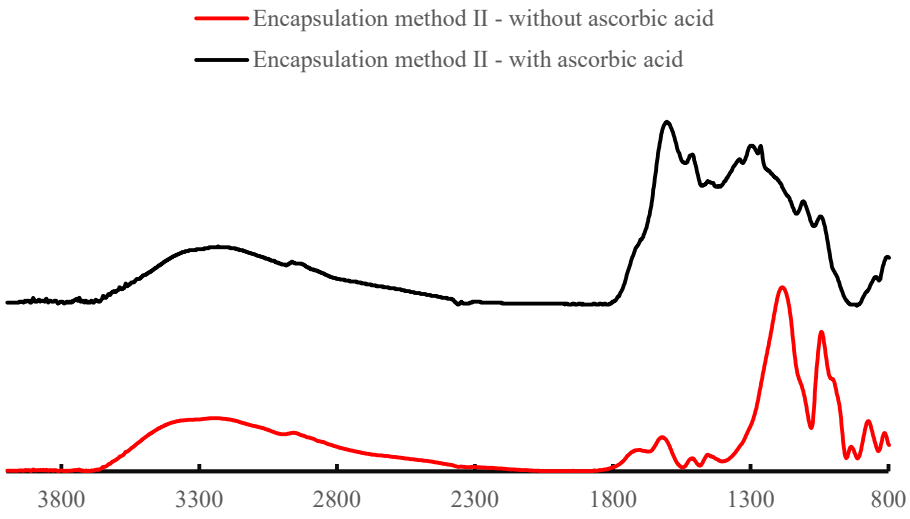

Figure 51: The FTIR spectra of sample prepared by the encapsulation method II, without using ascorbic acid and sample prepared by the encapsulation method II, while using ascorbic acid.

6 CONCLUSION

Successful and reproducible one-step selenium nanoparticles synthesis and their encapsulation via self-assembly polymerization of dopamine is the main and unique result of this thesis. The potential in use of polydopamine shell lies in stabilizing SeNPs, reducing their cytotoxicity andcompensating the loss of antibacterial properties of SeNPs after encapsulation due to the poly(dopamine) antibacterial properties. Moreover, the encapsulation technique is easily feasible and biocompatible.

The proposed work proves that the pH level has a big influence on dopamine self-assembly polymerization. Two methods of encapsulation are described in the experimental part. The results from the thesis showed, that lowering the water content during encapsulation process have no significant advantages, in some cases it brought more aggregates to the final product. Reliable method for concentration determination of selenium nanoparticles using UV-VIS was designed. Selenium nanoparticles were studied on scanning transmission electron microscope and Fourier-transformed infrared spectroscope. Chitosan, which generally stabilized selenium nanoparticles caused unwanted aggregation, by integrating with poly(dopamine) during encapsulation. Selenium nanoparticles stabilized by poly (sodium 4-styrenesulfonate) came out to be more suitable for encapsulation, because this protecting agent provided less interactions with poly(dopamine). Which makes the aggregates less frequent. On the other hand, the polydopamine shell was not stable on these nanoparticles. After just 24 hours in refrigerator the poly(dopamine) shells started to disintegrate. Encapsulation method II without ascorbic acid provided nicely encapsulated stable nanoparticles, smaller than 580 nm. This work proved stability of this sample throughout 48-hour time period.

When taking all these results into consideration, the two-steps encapsulation method I providing selenium nanoparticles stabilized by poly(sodium 4-styrenesulfonate) with higher than 15 ml water content resulting in size of SeNPS ranging from 108 to 571.5 nm and the one-step encapsulation method II without using ascorbic acid producing SeNPs with the size ranging from 74.5 to 228 nm seem to be most successful and worth methods being further studied in terms of nanoparticles biocompatibility and antibacterial properties.

7 REFERENCES

[1] ENGEL, Elisabeth, Alexandra MICHIARDI, Melba NAVARRO, Damien LACROIX a Josep A. PLANELL, 2008. Nanotechnology in regenerative medicine: the materials side. *Trends in Biotechnology*. **26**(1), 39-47.

[2] MAO, Angelo S., David J. MOONEY, Melba NAVARRO, Damien LACROIX a Josep A. PLANELL, 2015. Regenerative medicine: Current therapies and future directions. *Proceedings of the National Academy of Sciences*. **112**(47), 14452-14459.

[3] FEHER, Joseph, David J. MOONEY, Melba NAVARRO, Damien LACROIX a Josep A. PLANELL, 2017. Cell Signaling: Current therapies and future directions. *Quantitative Human Physiology*. Elsevier, 2017, **112**(47), 205-217.

[4] WORGALL, Stefan, Ronald G. CRYSTAL, Melba NAVARRO, Damien LACROIX a Josep A. PLANELL, 2014. Gene Therapy: Current therapies and future directions. *Principles of Tissue Engineering*. Elsevier, 2014, **112**(47), 657-686.

[5] FURTH, Mark E., Anthony ATALA, Melba NAVARRO, Damien LACROIX a Josep A. PLANELL, 2014. Tissue Engineering: Current therapies and future directions. *Principles of Tissue Engineering*. Elsevier, 2014, **112**(47), 83-123.

[6] MURUGAN, Ramalingam a Seeram RAMAKRISHNA, 2006. Nano-Featured Scaffolds for Tissue Engineering: A Review of Spinning Methodologies. *Tissue Engineering*. **12**(3), 435-447.

[7] KUMAR, Pawan a Anil SINDHU, 2018. Materials for Tissue Engineering: A Review of Spinning Methodologies. *Advances in Animal Biotechnology and its Applications*. Singapore: Springer Singapore, 2018-05-30, **12**(3), 357-370.

[8] ROCO, Mihail C, 2003. Nanotechnology: convergence with modern biology and medicine. *Current Opinion in Biotechnology*. **14**(3), 337-346.

[9] ALOPAEUS, Julia F., Marie HELLFRITZSCH, Tobias GUTOWSKI, Regina SCHERLIESS, Andreia ALMEIDA, Bruno SARMENTO, Nataša ŠKALKO-BASNET a Ingunn THO, 2020. Mucoadhesive buccal films based on a graft co-polymer – A mucin-retentive hydrogel scaffold. *European Journal of Pharmaceutical Sciences*. **142**.

[10] PAGANO, Cinzia, Maria Rachele CECCARINI, Paola CALARCO, Stefania SCUOTA, Carmela CONTE, Sara PRIMAVILLA, Maurizio RICCI a Luana PERIOLI, 2019. Bioadhesive polymeric films based on usnic acid for burn wound treatment: Antibacterial and cytotoxicity studies. *Colloids and Surfaces B: Biointerfaces*. **178**, 488-499.

[11] HARAGUCHI, Kazutoshi, Toru TAKEHISA, Simon FAN, Stefania SCUOTA, Carmela CONTE, Sara PRIMAVILLA, Maurizio RICCI a Luana PERIOLI, 2002. Effects of Clay Content on the Properties of Nanocomposite Hydrogels Composed of Poly(N-isopropylacrylamide) and Clay: Antibacterial and cytotoxicity studies. *Macromolecules*. **35**(27), 10162-10171.

[12] DENRY, Isabelle, Ourania-Menti GOUDOURI, Douglas C. FREDERICKS, Adil AKKOUCH, Michael R. ACEVEDO, Julie A. HOLLOWAY, Maurizio RICCI a Luana PERIOLI, 2018. Strontium-releasing fluorapatite glass-ceramic scaffolds: Structural

characterization and in vivo performance. *Acta Biomaterialia*. **75**(27), 463-471.

[13] ABAD-JAVIER, M.E., M. CAJERO-JUÁREZ, R.E. NUÑEZ-ANITA, M.E. CONTRERAS-GARCÍA, Michael R. ACEVEDO, Julie A. HOLLOWAY, Maurizio RICCI a Luana PERIOLI, 2019. Effect of collagen type I and vitamin D3 functionalization of biomimetic bioglass scaffolds on hydroxyapatite condensation: Structural characterization and in vivo performance. *Journal of the European Ceramic Society*. **39**(12), 3505-3512.

[14] DENRY, Isabelle, Ourania-Menti GOUDOURI, Douglas C. FREDERICKS, Adil AKKOUCH, Michael R. ACEVEDO, Julie A. HOLLOWAY, Maurizio RICCI a Luana PERIOLI, 2018. Strontium-releasing fluorapatite glass-ceramic scaffolds: Structural characterization and in vivo performance. *Acta Biomaterialia*. **75**(12), 463-471.

[15] ZACCARIA, Sabrina, Ronald C. VAN GAAL, Martijn RIOOL, Sebastian A. J. ZAAT, Patricia Y. W. DANKERS, Julie A. HOLLOWAY, Maurizio RICCI a Luana PERIOLI, 2018. Antimicrobial peptide modification of biomaterials using supramolecular additives: Structural characterization and in vivo performance. *Journal of Polymer Science Part A: Polymer Chemistry*. **56**(17), 1926-1934.

[16] SAMPRASIT, Wipada, Benchawan CHAMSAI, Sukanya SETTHARAKSA, Praneet OPANASOPIT, Patricia Y. W. DANKERS, Julie A. HOLLOWAY, Maurizio RICCI a Luana PERIOLI, 2020. Synergistic antibacterial activity of alpha mangostin and resveratrol loaded polymer-based films against bacteria infected wound: Structural characterization and in vivo performance. *Journal of Drug Delivery Science and Technology*. **57**(17), 1926-1934.

[17] PAGANO, Cinzia, Maria Rachele CECCARINI, Paola CALARCO, Stefania SCUOTA, Carmela CONTE, Sara PRIMAVILLA, Maurizio RICCI a Luana PERIOLI, 2019. Bioadhesive polymeric films based on usnic acid for burn wound treatment: Antibacterial and cytotoxicity studies. *Colloids and Surfaces B: Biointerfaces*. **178**(17), 488-499.

[18] DREXLER, K. E., C. PETERSON a G. PERGAMIT, 1991. *The Unbounding Future: the Nanotechnology Revolution*. New York: William Morrow and Company.

[19] SANCHEZ, Florence a Konstantin SOBOLEV, 2010. Nanotechnology in concrete – A review: convergence with modern biology and medicine. *Construction and Building Materials*. **24**(11), 2060-2071.

[20] JEEVANANDAM, Jaison, Ahmed BARHOUM, Yen S CHAN, Alain DUFRESNE a Michael K DANQUAH, 2018. Review on nanoparticles and nanostructured materials: history, sources, toxicity and regulations. *Beilstein Journal of Nanotechnology*. **9**, 1050-1074.

[21] NAGARAJAN, R., 2008. Nanoparticles: Building Blocks for Nanotechnology. *Nanoparticles: Synthesis, Stabilization, Passivation, and Functionalization*. Washington, DC: American Chemical Society, 2008-09-19, 2-14. ACS Symposium Series.

[22] KHAN, Ibrahim, Khalid SAEED, Idrees KHAN, Alain DUFRESNE a Michael K DANQUAH, 2019. Nanoparticles: Properties, applications and toxicities. *Arabian Journal of Chemistry*. **12**(7), 908-931.

[23] LIU, Yanjing, Richard. O. CLAUS, Lin Lin ZHAO, George C. SCHATZ a E. P. GIANNELIS, 1997. Blue Light Emitting Nanosized TiO 2 Colloids: The Influence of Size,

Shape, and Dielectric Environment. *Journal of the American Chemical Society*. Washington, DC: American Chemical Society, 2008-09-19, **119**(22), 5273-5274. ACS Symposium Series.

[24] BOLAÑOS, Karen, Marcelo J KOGAN a Eyleen ARAYA, 2019. Capping gold nanoparticles with albumin to improve their biomedical properties . *International Journal of Nanomedicine*. **14**, 6387-6406.

[25] PERÁN, Macarena, María A. GARCÍA, Elena LÓPEZ-RUIZ, Milán BUSTAMANTE, Gema JIMÉNEZ, Roberto MADEDDU a Juan A. MARCHAL, 2012. Functionalized Nanostructures with Application in Regenerative Medicine: An Overview on Different Biological Systems. *International Journal of Molecular Sciences*. Dordrecht: Springer Netherlands, 2013-11-18, **13**(3), 3847-3886. Metal Ions in Life Sciences.

[26] MOFFAT, Kristen L., Anne S.-P. KWEI, Jeffrey P. SPALAZZI, Stephen B. DOTY, William N. LEVINE, Helen H. LU, Maurizio RICCI a Luana PERIOLI. Novel Nanofiber-Based Scaffold for Rotator Cuff Repair and Augmentation: Antibacterial and cytotoxicity studies. *Tissue Engineering Part A*. 2009, **15**(1), 115-126.

[27] QIAN, Saibo, Zhilin YAN, Yongjie XU, Huaping TAN, Yong CHEN, Zhonghua LING, Xiaohong NIU a Luana PERIOLI. Carbon nanotubes as electrophysiological building blocks for a bioactive cell scaffold through biological assembly to induce osteogenesis: Antibacterial and cytotoxicity studies. *RSC Advances*. 2019, **9**(21), 12001-12009.

[28] GABAY, Tamir, Eyal JAKOBS, Eshel BEN-JACOB, Yael HANEIN, Yong CHEN, Zhonghua LING, Xiaohong NIU a Luana PERIOLI. Engineered self-organization of neural networks using carbon nanotube clusters: Antibacterial and cytotoxicity studies. *Physica A: Statistical Mechanics and its Applications*. 2005, **350**(2-4), 611-621.

[29] KWAN, Karen H.L., Xuelai LIU, Michael K.T. TO, Kelvin W.K. YEUNG, Chi-ming HO, Kenneth K.Y. WONG a Juan A. MARCHAL, 2011. Modulation of collagen alignment by silver nanoparticles results in better mechanical properties in wound healing: An Overview on Different Biological Systems. *Nanomedicine: Nanotechnology, Biology and Medicine*. Dordrecht: Springer Netherlands, 2013-11-18, **7**(4), 497-504. Metal Ions in Life Sciences.

[30] KENNEDY, Laura C., Lissett R. BICKFORD, Nastassja A. LEWINSKI, et al. A New Era for Cancer Treatment: Gold-Nanoparticle-Mediated Thermal Therapies. *Small*. 2011, **7**(2), 169-183.

[31] BRAZEL, Christopher S., 2009. Magnetothermally-responsive Nanomaterials: Combining Magnetic Nanostructures and Thermally-Sensitive Polymers for Triggered Drug Release. *Pharmaceutical Research*. **26**(3), 644-656.

[32] WOLFBEIS, Otto S., James W. LILLARD, Joana GOMES, et al. An overview of nanoparticles commonly used in fluorescent bioimaging: A perspective. *Chemical Society Reviews*. 2015, **44**(14), 4743-4768.

[33] WANG, Linlin, Chen HU a Longquan SHAO, 2017. The antimicrobial activity of nanoparticles: present situation and prospects for the future. *International Journal of Nanomedicine*. **12**(3), 1227-1249.

[34] MATAI, Ishita, Abhay SACHDEV, Poornima DUBEY, S. UDAY KUMAR, Bharat BHUSHAN, P. GOPINATH a Juan A. MARCHAL. Antibacterial activity and mechanism of Ag–ZnO nanocomposite on S. aureus and GFP-expressing antibiotic resistant E. coli: An Overview on Different Biological Systems. *Colloids and Surfaces B: Biointerfaces*. Dordrecht: Springer Netherlands, 2014, 2013-11-18, **115**(4), 359-367. Metal Ions in Life Sciences.

[35] HAJIPOUR, Mohammad J., Katharina M. FROMM, Ali AKBAR ASHKARRAN, et al. Antibacterial properties of nanoparticles: present situation and prospects for the future. *Trends in Biotechnology*. 2012, **30**(10), 499-511.

[36] MORITZ, Michał, Małgorzata GESZKE-MORITZ, Eshel BEN-JACOB, Yael HANEIN, Yong CHEN, Zhonghua LING, Xiaohong NIU a Luana PERIOLI. The newest achievements in synthesis, immobilization and practical applications of antibacterial nanoparticles: Antibacterial and cytotoxicity studies. *Chemical Engineering Journal*. 2013, **228**(10), 596-613.

[37] MAHMOODI, Shirin, Asghar ELMI, Somayeh HALLAJ NEZHADI, Yael HANEIN, Yong CHEN, Zhonghua LING, Xiaohong NIU a Luana PERIOLI. Copper Nanoparticles as Antibacterial Agents: Antibacterial and cytotoxicity studies. *Chemical Engineering Journal*. 2018, **06**(01), 596-613.

[38] LV, Pengzhao, Lianjie ZHU, Yanmiao YU, Wenwen WANG, Guokai LIU, Hongguang LU, Xiaohong NIU a Luana PERIOLI. Effect of NaOH concentration on antibacterial activities of Cu nanoparticles and the antibacterial mechanism: Antibacterial and cytotoxicity studies. *Materials Science and Engineering: C*. 2020, **110**(01), 596-613.

[39] MARAMBIO-JONES, Catalina, Eric M. V. HOEK, Joana GOMES, et al. A review of the antibacterial effects of silver nanomaterials and potential implications for human health and the environment: A perspective. *Journal of Nanoparticle Research*. 2010, **12**(5), 1531-1551.

[40] INGLE, Avinash, Aniket GADE, Sebastien PIERRAT, et al. Mycosynthesis of Silver Nanoparticles Using the Fungus Fusarium acuminatum and its Activity Against Some Human Pathogenic Bacteria: A perspective. *Current Nanoscience*. 2008, **4**(2), 141-144.

[41] KENNEDY, Laura C., Lissett R. BICKFORD, Nastassja A. LEWINSKI, et al. A New Era for Cancer Treatment: Gold-Nanoparticle-Mediated Thermal Therapies. *Small*. 2011, **7**(2), 169-183.

[42] BINDHU, M.R., M. UMADEVI, Robert J. HUGHES, Robert J. MOORE, James CHAPMAN, P. GOPINATH a Juan A. MARCHAL. Silver and gold nanoparticles for sensor and antibacterial applications: An Overview on Different Biological Systems. *Spectrochimica Acta Part A: Molecular and Biomolecular Spectroscopy*. Dordrecht: Springer Netherlands, 2014, 2013-11-18, **128**(11), 37-45. Metal Ions in Life Sciences.

[43] ZHOU, Yan, Ying KONG, Subrata KUNDU, Jeffrey D CIRILLO, Hong LIANG, P. GOPINATH a Juan A. MARCHAL. Antibacterial activities of gold and silver nanoparticles against Escherichia coli and bacillus Calmette-Guérin: An Overview on Different Biological Systems. *Journal of Nanobiotechnology*. Dordrecht: Springer Netherlands, 2012, 2013-11-

18, **10**(1), 37-45. Metal Ions in Life Sciences.

[44] ASHARANI, P. V., Grace LOW KAH MUN, Manoor Prakash HANDE, et al., 2009. Cytotoxicity and Genotoxicity of Silver Nanoparticles in Human Cells: An Overview on Different Biological Systems. *ACS Nano*. Dordrecht: Springer Netherlands, 2013-11-18, **3**(2), 279-290. Metal Ions in Life Sciences.

[45] SUNG, Jae Hyuck, Jun Ho JI, Jin Uk YOON, et al. Lung Function Changes in Sprague-Dawley Rats After Prolonged Inhalation Exposure to Silver Nanoparticles: Gold-Nanoparticle-Mediated Thermal Therapies. *Inhalation Toxicology*. 2008, **20**(6), 567-574.

[46] BRAYDICH-STOLLE, Laura, Saber HUSSAIN, John J. SCHLAGER, et al. In Vitro Cytotoxicity of Nanoparticles in Mammalian Germline Stem Cells: Gold-Nanoparticle-Mediated Thermal Therapies. *Toxicological Sciences*. 2005, **88**(2), 412-419.

[47] SHARMA, Deepali, Suvardhan KANCHI, Krishna BISETTY, et al. Biogenic synthesis of nanoparticles: A review. *Arabian Journal of Chemistry*. 2015, **46**(02), 223-233.

[48] NGUYEN, Nhu-Y Thi, Nathaniel GRELLING, Cheyann Lee WETTELAND, Romeo ROSARIO, Huinan LIU, Hongguang LU, Xiaohong NIU a Luana PERIOLI. Antimicrobial Activities and Mechanisms of Magnesium Oxide Nanoparticles (nMgO) against Pathogenic Bacteria, Yeasts, and Biofilms: Antibacterial and cytotoxicity studies. *Scientific Reports*. 2018, **8**(1), 596-613.

[49] WEBSTER, Thomas J, Iustin SEIL, Panagiota LOUKA, et al. Antimicrobial applications of nanotechnology: methods and literature. *International Journal of Nanomedicine*. 2010, **7**(9), 1063-1077.

[50] RASMUSSEN, John W, Ezequiel MARTINEZ, Panagiota LOUKA, et al. Zinc oxide nanoparticles for selective destruction of tumor cells and potential for drug delivery applications: Synergistic effects of shape and surface functionalization on micromotility of epithelial cells. *Expert Opinion on Drug Delivery*. 2010, **7**(9), 1063-1077.

[51] KUROKAWA, Suguru, Marla J. BERRY, Enrica PESSIONE a Vini GAUTAM, 2013. Selenium. Role of the Essential Metalloid in Health: An Overview on Different Biological Systems. *Interrelations between Essential Metal Ions and Human Diseases*. Dordrecht: Springer Netherlands, 2013-11-18, **15**(6), 499-534. Metal Ions in Life Sciences.

[52] SAKR, Tamer M., M. KORANY, Kattesh V. KATTI, et al. Selenium nanomaterials in biomedicine—An overview of new opportunities in nanomedicine of selenium: methods and literature. *Journal of Drug Delivery Science and Technology*. 2018, **46**(02), 223-233.

[53] SONKUSRE, Praveen, M. KORANY, Kattesh V. KATTI, et al. Improved Extraction of Intracellular Biogenic Selenium Nanoparticles and their Specificity for Cancer Chemoprevention: methods and literature. *Journal of Drug Delivery Science and Technology*. 2014, **05**(02), 223-233.

[54] NGUYEN, Trang H.D., Bongkosh VARDHANABHUTI, Mengshi LIN a Azlin MUSTAPHA, 2017. Antibacterial properties of selenium nanoparticles and their toxicity to Caco-2 cells: An Overview on Different Biological Systems. *Food Control*. Dordrecht: Springer Netherlands, 2013-11-18, **77**(6), 17-24. Metal Ions in Life Sciences.

[55] KHIRALLA, Ghada M., Bahig A. EL-DEEB, Mengshi LIN a Azlin MUSTAPHA, 2015. Antimicrobial and antibiofilm effects of selenium nanoparticles on some foodborne pathogens: An Overview on Different Biological Systems. *LWT - Food Science and*

Technology. Dordrecht: Springer Netherlands, 2013-11-18, **63**(2), 1001-1007. Metal Ions in Life Sciences.

[56] AVENDAÑO, Roberto, Nefertiti CHAVES, Paola FUENTES, Ethel SÁNCHEZ, Jose I. JIMÉNEZ a Max CHAVARRÍA, 2016. Production of selenium nanoparticles in Pseudomonas putida KT2440: An Overview on Different Biological Systems. *Scientific Reports*. Dordrecht: Springer Netherlands, 2013-11-18, **6**(1), 1001-1007. Metal Ions in Life Sciences.

[57] HOSNEDLOVA, Bozena, Marta KEPINSKA, Sylvie SKALICKOVA, et al. Nano-selenium and its nanomedicine applications: a critical review. *International Journal of Nanomedicine*. 2018, **13**(1), 2107-2128.

[58] GANGADOO, Sheeana, Dragana STANLEY, Robert J. HUGHES, Robert J. MOORE, James CHAPMAN, P. GOPINATH a Juan A. MARCHAL. The synthesis and characterisation of highly stable and reproducible selenium nanoparticles: An Overview on Different Biological Systems. *Inorganic and Nano-Metal Chemistry*. Dordrecht: Springer Netherlands, 2017, 2013-11-18, **47**(11), 1568-1576. Metal Ions in Life Sciences.

[59] LIONG, Monty, Bryan FRANCE, Kenneth A. BRADLEY, et al. Antimicrobial Activity of Silver Nanocrystals Encapsulated in Mesoporous Silica Nanoparticles: A review. *Advanced Materials*. 2009, **21**(17), 1684-1689.

[60] THORAT, Nanasaheb D., Raghvendra A. BOHARA, Mohamed Radzi NOOR, et al. Effective Cancer Theranostics with Polymer Encapsulated Superparamagnetic Nanoparticles: A review. *Advanced Materials*. 2016, **3**(7), 1332-1340.

[61] ZHANG, Shu, Yangchao LUO, Huawei ZENG, et al. Encapsulation of selenium in chitosan nanoparticles improves selenium availability and protects cells from selenium-induced DNA damage response: Combined Effects of Magnetic Hyperthermia and Controlled Drug Release. *The Journal of Nutritional Biochemistry*. 2011, **22**(12), 1137-1142.

[62] LADJ, Rachid, Ahmad BITAR, Mohamed M. EISSA, et al. Polymer encapsulation of inorganic nanoparticles for biomedical applications: Combined Effects of Magnetic Hyperthermia and Controlled Drug Release. *International Journal of Pharmaceutics*. 2013, **458**(1), 230-241.

[63] FANG, Zhongxiang, Bhesh BHANDARI, C.C. WANG, et al. Encapsulation of polyphenols – a review: Combined Effects of Magnetic Hyperthermia and Controlled Drug Release. *Advanced Materials*. 2010, **21**(10), 510-523.

[64] OLIVEIRA, Mariana B., Javad HATAMI a João F. MANO, 2016. Coating Strategies Using Layer-by-layer Deposition for Cell Encapsulation. *Chemistry - An Asian Journal*. **11**(12), 1753-1764.

[65] FOLEY, P., 2009. Dopamine in Perspective. *Encyclopedia of Neuroscience*. Elsevier, 2009, 563-570.

[66] LIEBSCHER, Jürgen, 2019. Chemistry of Polydopamine - Scope, Variation, and Limitation. *European Journal of Organic Chemistry*. **2019**(31-32), 4976-4994.

[67] BINNS, F., J. A. G. KING, S. N. MISHRA, A. PERCIVAL, N. C. ROBSON, G. A. SWAN a A. WAGGOTT, 1970. Studies related to the chemistry of melanins. Part XIII. Studies on the structure of dopamine-melanin. *Journal of the Chemical Society C: Organic*. (15).

[68] MIKSA, Beata, Eyal JAKOBS, Eshel BEN-JACOB, Yael HANEIN, Yong CHEN,

Zhonghua LING, Xiaohong NIU a Luana PERIOLI. Fluorescent Dyes Used in Polymer Carriers as Imaging Agents in Anticancer Therapy: Antibacterial and cytotoxicity studies. *Medicinal chemistry*. 2016, **6**(10), 611-621.

[69] LEE, H., S. M. DELLATORE, W. M. MILLER a P. B. MESSERSMITH. Mussel-Inspired Surface Chemistry for Multifunctional Coatings. *Science*. 2007, **318**(5849), 426-430.

[70] RYU, Ji Hyun, Phillip B. MESSERSMITH, Haeshin LEE a P. B. MESSERSMITH. Polydopamine Surface Chemistry: A Decade of Discovery. *Science*. 2018, **10**(9), 7523-7540.

[71] LIU, Dongdong, Liyi MA, Lidong LIU, et al. Polydopamine-Encapsulated Fe 3 O 4 with an Adsorbed HSP70 Inhibitor for Improved Photothermal Inactivation of Bacteria: An Overview on Different Biological Systems. *Journal of Nanobiotechnology*. Dordrecht: Springer Netherlands, 2016, 2013-11-18, **8**(37), 24455-24462. Metal Ions in Life Sciences.

[72] SUN, Changlong, Mingxia GAO, Xiangmin ZHANG, et al. Surface-enhanced Raman scattering (SERS) imaging-guided real-time photothermal ablation of target cancer cells using polydopamine-encapsulated gold nanorods as multifunctional agents: An Overview on Different Biological Systems. *Analytical and Bioanalytical Chemistry*. Dordrecht: Springer Netherlands, 2017, 2013-11-18, **409**(20), 4915-4926. Metal Ions in Life Sciences.

[73] JUNG, Hak-Sung, Kyung-Jin CHO, Yeonee SEOL, et al. Polydopamine Encapsulation of Fluorescent Nanodiamonds for Biomedical Applications: An Overview on Different Biological Systems. *Advanced Functional Materials*. Dordrecht: Springer Netherlands, 2018, 2013-11-18, **28**(33), 24455-24462. Metal Ions in Life Sciences.

[74] ZHU, Jinjin, Zhu WANG, Xiaolin XU, et al. Polydopamine-Encapsulated Perfluorocarbon for Ultrasound Contrast Imaging and Photothermal Therapy: An Overview on Different Biological Systems. *Molecular Pharmaceutics*. Dordrecht: Springer Netherlands, 2020, 2013-11-18, **17**(3), 817-826. Metal Ions in Life Sciences.

[75] *Komplex biopolymerní látky s nanočásticemi selenu a antibiotickými léčivy s antibakteriálním účinkem*. 2014. The Czech Republic. CZ 26981 U1. Registrated 26.5.2014.

[76] ZHAO, Xing Guan, Kyung-Jun HWANG, Dongoh LEE, Taemin KIM a Namsu KIM, 2018. Enhanced mechanical properties of self-polymerized polydopamine-coated recycled PLA filament used in 3D printing. *Applied Surface Science*. **441**, 381-387.

8 LIST OF ABBREVIATIONS

AA	Ascorbic acid
ATR	Attenuated total reflection
AuNP	Gold nanoparticles
AuNR	Gold nanorods
Cu(II)	Cupric ions
DCM	Dichlormethane
DNA	Deoxyribonucleic acid
FDA	Food and Drug Administration
Fe_3O_4	Ferrosoferric oxide
FTIR	Fourier-transform infrared spectroscopy
$KMnO_4$	Potassium permanganate
MgO	Magnesium oxide
NIR	Near-infrared spectroscopy
NP	Nanoparticles
PAH	Polyelectrolyte
PDA	Polydopamine
PEG	Polyethylene glycol
PES	Photoelectron spectroscopy
PFC	Perfluorinated compound
SE	Secondary-electron detector
SeCh	Selenium nanoparticles stabilized by chitosan
SEM	Scanning electron microscope
SeNPs	Selenium nanoparticles
SePSSS	Selenium nanoparticles stabilized by poly (sodium 4-styrenesulfonate)
SERS	Surface-enhanced Raman scattering
STEM	Scanning transmission electron microscope
UV	Ultraviolet
VIS	Visible
ZnO	Zinc oxide

9 LIST OF FIGURES

Figure 1: Flow chart for the classification of biomaterials with examples. 10
Figure 2: Schematic illustration of nanostructure shapes [24]. 12
Figure 3: SE images of aligned (A) and unaligned (B) nanofiber scaffolds [26]. 12
Figure 4: Schematic illustration of the carbon nanotube gel scaffold preparation [27]. 13
Figure 5: Optical image islands of carbon nanotubes (a). SEM image of island coated by nanotubes (b).[28] 13
Figure 6: Inverted microscope images of on carbon nanotube islands organized neuronal system. Cluster formations were studied after 96 hours (a), 128 hours (b), and 150 hours (c). With time, the islands became more connected.[28] 14
Figure 7: The classification of antibacterial nanoparticles in terms of chemical composition [36]. 16
Figure 8: Schematic illustration of antibacterial mechanism of copper nanoparticles to bacteria.[38] 17
Figure 9: The impact of gold nanoparticles capped by PAH on bacterial cell [43](modified) 18
Figure 10: SEM images of Escherichia coli, showing its morphology after cultured with 0-1.2 mg/ml of MgO nanoparticles for 24 hours [48]..... 19
Figure 11: Scheme describing the main effects of selenium nanoparticles [57]..... 20
Figure 12: Dopamine autoxidation scheme..... 22
Figure 13: Impact of different pH levels on polydopamine. 23
Figure 14: Nanoparticle preparation and encapsulation[71](modified)..... 24
Figure 15: Encapsulation of gold nanorods in polydopamine and its utilization in cancer treatment[72](modified)..... 24
Figure 16: Perfluorocarbon nanodroplets encapsulated in polydopamine, stabilized by polyethylene glycol[74](modified) 25
Figure 17: Schematic description of nanoparticle preparation and encapsulation method I ... 30
Figure 18: Schematic description of nanoparticle preparation and encapsulation method II. . 32
Figure 19: The calibration line for selenium nanoparticles..... 35
Figure 20: The absorbation spectrum of selenium nanoparticles with concentration 125 nM. 35
Figure 21: SE and STEM images of selenium nanoparticles stabilized by chitosan. 36
Figure 22: Size distribution of selenium nanoparticles stabilized by chitosan. 36
Figure 23: SE and STEM images of selenium nanoparticles stabilized by poly (sodium 4-styrenesulfonate) supernatant. 37
Figure 24: Size distribution of selenium nanoparticles stabilized in poly (sodium 4-styrenesulfonate) supernatant. 38
Figure 25: SE and STEM images of selenium nanoparticles stabilized by poly (sodium 4-styrenesulfonate) precipitate. 38
Figure 26: Size distribution of selenium nanoparticles stabilized

by poly (sodium 4-styrenesulfonate) precipitate. 39
Figure 27: The boxplot representing calculated particle sizes of selenium nanoparticles stabilized by PSSS in supernatant, precipitate, and selenium nanoparticles stabilized by chitosan. 40
Figure 28: FTIR spectrum of selenium nanoparticles stabilized by chitosan. 41
Figure 29: FTIR spectrum of selenium nanoparticles stabilized by poly (sodium 4-styrenesulfonate). 41
Figure 30: Samples prepared to undergo the polymerization, on the left side sample without selenium nanoparticles present, on the right side samples containing selenium nanoparticles. 42
Figure 31:The SE and STEM images of obtained polydopamine. 43
Figure 32:The SE and STEM images of selenium nanoparticles stabilized by chitosan and encapsulated in polydopamine using the encapsulation method I. 43
Figure 33:The SE and STEM images of selenium nanoparticles stabilized by chitosan and encapsulated in polydopamine using the encapsulation method I, with lowered water content. 44
Figure 34: The SE and STEM images of selenium nanoparticles stabilized by poly (sodium 4-styrenesulfonate) and encapsulated in polydopamine using the encapsulation method I. 45
Figure 35: The size distribution of encapsulated selenium nanoparticles stabilized by poly (sodium 4-styrenesulfonate, prepared according to encapsulation method I. 45
Figure 36: The SE image of encapsulated selenium nanoparticles stabilized by poly (sodium 4-styrenesulfonate), prepared according to encapsulation method Iafter 24 hours in the refrigerator. 46
Figure 37: The SE and STEM images of encapsulated selenium nanoparticles stabilized by poly (sodium 4-styrenesulfonate), prepared according to encapsulation method I after 48 hours in the refrigerator. 46
Figure 38: The SE and STEM images of selenium nanoparticles stabilized by poly (sodium 4-styrenesulfonate) and encapsulated in polydopamine using encapsulation method I, with lowered water content. 47
Figure 39: The size distribution of encapsulated selenium nanoparticles stabilized by poly (sodium 4-styrenesulfonate), prepared according to encapsulation method I, with lowered water content. 47
Figure 40: The boxplot containing calculated surfaces of selenium nanoparticles stabilized by PSSS encapsulated in polydopamine using encapsulation method I. 48
Figure 41: The SE and STEM images of encapsulated selenium nanoparticles prepared by the encapsulation method II, while not using the ascorbic acid. 49
Figure 42: The size distribution of encapsulated selenium nanoparticles prepared by the encapsulation method II, while not using the ascorbic acid. 49
Figure 43: The SE image of PDA_4D sample after 48 hours in refrigerator. 50

Figure 44: The SE and STEM images of encapsulated selenium nanoparticles prepared by the encapsulation method II, while using the ascorbic acid. 50
Figure 45: The size distribution histogram of encapsulated selenium nanoparticles prepared by the encapsulation method II, while using ascorbic acid. 51
Figure 46: The boxplot of containing calculated surfaces of encapsulated selenium nanoparticles using encapsulation method II. 51
Figure 47: The FTIR spectra of dopamine and polydopamine. 52
Figure 48: The FTIR spectra of selenium nanoparticles stabilized by chitosan and selenium nanoparticles stabilized by chitosan encapsulated according to encapsulation method I. 53
Figure 49: Description of dopamine polymerization process.[76] 54
Figure 50: The FTIR spectra of pure selenium nanoparticles stabilized by poly (sodium 4-styrenesulfonate), encapsulated selenium nanoparticles stabilized by poly (sodium 4-styrenesulfonate) with normal water content and encapsulated selenium nanoparticles stabilized by poly (sodium 4-styrenesulfonate) with lowered water content. ... 55
Figure 51: The FTIR spectra of sample prepared by the encapsulation method II, without using ascorbic acid and sample prepared by the encapsulation method II, while using ascorbic acid. 56

10 LIST OF TABLES

Table 1: Summarisation of additives used in tissue regeneration. 11
Table 2: Sample preparation description. SeCh – selenium nanoparticles stabilized by chitosan, SePSSS – selenium nanoparticles stabilized by poly (sodium 4-styrenesulfonate). 31
Table 3: Preparation of last two samples. 32
Table 4: Results of titration using $KMnO_4$ 34
Table 5: The absorptions of calibration line at 269 nm. 35
Table 6: Colour changes during encapsulation. 42